Advances in Nano Research, *Vol. 11, No. 5 (2021) 521-536*
https://doi.org/10.12989/anr.2021.11.5.521

Metal-organic framework films functionalized with nonionic conjugated polythiophenes for visual detection of PAHs

Salah M. Tawfik[1] and Yong-Ill Lee*[2]

[1]*Department of Petrochemicals, Egyptian Petroleum Research Institute (EPRI) Nasr City, Cairo 11727, Egypt*
[2]*Department of Materials Convergence and System Engineering, Changwon National University, Changwon 51140, Republic of Korea*

(*Received July 12, 2021, Revised September 29, 2021, Accepted October 6, 2021*)

Abstract. Natural and anthropogenic activities lead to the generation of polycyclic aromatic hydrocarbons (PAHs), persistent contaminants that adversely affect the environment and public health. However, highly sensitive, fast, and portable techniques for the detection of PAHs remain a technological challenge. The rapid analysis of urinary levels of 1-hydroxypyrene (1-HP) would enable PAH carcinogens to be measured using biomonitoring techniques. Here, we demonstrate biocompatible, easy-to-use, and portable sensors based on novel π-conjugated metal-organic frameworks (MOFs) for the detection of 1-HP. These sensors were developed by incorporating nonionic conjugated polythiophenes with a PLQY as high as 65% into lanthanide-MOFs (CP1-Eu-MOF and CP2-Eu-MOF) using an in-situ synthesis strategy. The emission of the sensors can be effectively quenched by 1-HP via hydrophobic, π–π stacking, and hydrogen bonding interactions. Significantly, the unique structure of CP2-Eu-MOF sensor displays superior performance with enhanced sensitivity (LOD ~1.02 pM) that is 1.63 times higher than that of CP1-Eu-MOF (LOD ~1.66 pM). More importantly, we successfully demonstrated the possibility of employing wax-printed paper in combination with a fast and cost-effective smartphone for rapid 1-HP detection. Moreover, portable sensory films were fabricated by incorporating CP2-Eu-MOF into a poly(vinylidene difluoride) (PVDF) matrix to produce CP2-Eu-MOF/PVDF films for the visual detection of 1-HP levels as low as 25 pM. Finally, the feasibility of successfully analyzing the levels of 1-HP in urine was verified by testing real urine samples with satisfactory recoveries of 94.1-103.5%. This method provides new pathways for the biomonitoring of polyaromatic environmental pollutants.
Keywords: conjugated polymers; fluorescent film; metal-organic framework nanostructures; PAHs sensor; Paper-smartphone devices; polycyclic aromatic hydrocarbons

1. Introduction

PAHs are a group of significant environmental pollutants that are generated by materials such as oil, coal, petrol, or wood as a result of incomplete combustion. Therefore, these pollutants can be present in the atmosphere, soil, water, and also in food consumed by humans (Abdel-Shafy and Mansour 2016, Habibullah-Al-Mamun *et al*. 2018, Jin *et al*. 2020, Li *et al*. 2022). PAHs are one of the main groups of toxic contaminants known as cancer-causing agents and in 2015, they were listed as the ninth most hazardous chemical with respect to human health. Human exposure to PAHs occurs via the inhalation of polluted air and the ingestion of polluted food and water (Oliveira *et al*. 2019). Owing to the bioaccumulation of PAHs as well as their stability and toxic effects on human health, several approaches for assessing PAH concentrations have been developed (Kim *et al*. 2013, Bansal and Kim 2015). The biomonitoring of specific biomarkers in urine is usually used as an effective index for human exposure to PAHs (Lin *et al*. 2021). For instance, 1-HP, a measurable urinary PAHs metabolite, is considered a general and accurate biomarker to indicate human exposure to PAH mixtures because 1-HP can reveal all possible sources, routes, and levels of exposure to PAHs (Wang *et al*. 2019). In many occupational settings, a clear correlation was also found between the level of PAH exposure and the level of excreted urinary 1-HP (Pruneda-Álvarez *et al*. 2016).

To date, conventional methods for the quantification of PAH have been used (Alekseenko *et al*. 2020, Gill *et al*. 2020, Omidi *et al*. 2020, Pang *et al*. 2020a). However, these approaches have drawbacks such as complex sample preparation, hazardous reagents, and are time-consuming to use. Recently, colorimetric (Hu *et al*. 2015), fluorescence (Hao and Yan 2017, Tropp *et al*. 2019, Nsibande and Forbes 2020, Xue *et al*. 2020), electrochemical (Shen *et al*. 2012a, b, Pang *et al*. 2019b, Li *et al*. 2020c) and surface-enhanced Raman scattering (Sur 2013, Gao *et al*. 2019, Li *et al*. 2019c, Ankamwar and Sur 2020, Castro-Grijalba *et al*. 2020) techniques were studied. Particularly, few methods-based fluorescence sensors for the determination of urinary levels of 1-HP with outstanding performance have been reported to date (Hao and Yan 2017, Sun *et al*. 2018, Zhou *et al*. 2018, Xue *et al*. 2019).

For example, Sun *et al*. (2018) incorporated a novel *p-tert*-butylsulfonylcalix[4]arene with a dinuclear terbium (III) complex resulting in detection limits of 4.20 μM. Furthermore, Zhou *et al*. (2018) constructed a mesoporous MOF based on zirconium/tetraethyl-(pyrene-1,3,6,8-tetrayl)

*Corresponding author, Professor,
E-mail: yilee@changwon.ac.kr

ISSN: 2287-237X (Print), 2287-2388 (Online)

tetrabenzoic acid and demonstrated 1-HP detection with detection limits of 48 nM. However, most of these methods have the disadvantage of low sensitivity, non-portability, and are too complicated to be used on site. In addition, the biocompatibility of these reported sensors has not been widely investigated. Therefore, the establishment of a sensitive, selective, quick, cost effective, portable, and environmentally friendly system for 1-HP detection is highly desired.

Polythiophenes (PT) and its derivatives are one of the most easily accessible and mass-producible candidates in terms of cost and commercial applications (Liang *et al*. 2019, Liang *et al*. 2020, Wang *et al*. 2020, Liu *et al*. 2021, Wang *et al*. 2021). Nonionic conjugated polythiophenes, which are π-conjugated polymers with nonionic side-chains, combine the excellent photoelectricity of conjugated polymers (CPs) with the high solubility and biocompatibility of nonionic polymers (Tawfik *et al*. 2018b, 2019, 2020, Ou *et al*. 2020). Because of their delocalized electronic structure, high extinction coefficients, and significant fluorescence emission properties, excellent sensitivity yields have been achieved compared with small fluorophores (Tawfik *et al*. 2018b, 2019, 2020). In our work, we exploited the advantages of CPs by replacing the conventional poorly soluble and toxic organic ligands by the new water soluble and biocompatible CP ligand to produce Eu-MOFs functionalized with conjugated polymers (CPs-Eu-MOFs). Metal−organic frameworks (MOFs) have been extensively explored as sensors owing to their quick, reusable, and reliable sensing characteristics (Ma *et al*. 2019, Phan-Quang *et al*. 2019, Soury *et al*. 2019, Luo *et al*. 2020, Wu *et al*. 2020a, b). MOFs have various advantageous structural characteristics in the form of a tunable pore structure, dimensions, and functionalities (Huang *et al*. 2017, Haldar *et al*. 2020, Kumar *et al*. 2021). The molecular design of the MOF pore system provides the opportunity to decorate the pores with a periodic range of chemical structures that enable molecular-level interactions between the framework and probe analytes to be controlled to provide selective sensing for specific analytes (Li *et al*. 2020a, Liu *et al*. 2020). Lanthanide MOFs (Ln-MOFs) have also been explored as ions (Xu and Yan 2017, Zeng *et al*. 2020), small organic compounds (Zhou *et al*. 2015, Xu *et al*. 2017), gases (Lin *et al*. 2016, Sava Gallis *et al*. 2019), explosives (Hu *et al*. 2014, Song *et al*. 2014), antibiotics (Zhang *et al*. 2017a, Li *et al*. 2020b), humidity (Chen *et al*. 2017, Zhang *et al*. 2017b) and temperature (Cui *et al*. 2015, Li *et al*. 2019b) sensors. Compared to conventional nonconjugated MOFs, few examples of MOFs with conjugated polythiophenes that integrate the π-conjugated framework, intrinsic porosity, and large surface area of MOFs with the unique features of CPs have been reported (Mallick *et al*. 2019, Zhou *et al*. 2021). This is the first time Eu-MOFs functionalized with nonionic conjugated polythiophenes have been fabricated into highly luminescent, flexible, and portable films for 1-HP detection.

Herein, we demonstrate a simple and effective method for 1-HP biomonitoring. The strategy was to combine Eu-MOFs and CPs, wherein the Eu-MOFs form the component that contributes intrinsic porosity and a large surface area, and the CPs function as a water soluble, biocompatible, π-conjugated molecular recognition ligands (Scheme 1). Compared to other fluorescence sensors for biomonitoring PAHs, this method has several advantages. (1) The incorporation of π-conjugated polythiophene ligands into Eu-MOFs could produce a strong synergistic effect and introduce intriguing photophysical and electrochemical properties into the framework, (2) The uniform hybridization of the Eu-MOFs based on two nonionic conjugated ligands was expected to produce a unique water soluble and biocompatible nanoscale sensor, (3) the high quantum yield of the ligands (65%) and ordered pore structure of MOFs (SBET = 1520 m^2 g^{-1}) enhance the sensitivity of the sensor, (4) In terms of 1-HP sensing, the sensors display outstanding performance with a low limit of detection (LOD) (1.02 pM) and fast response (20 min), (5) An advanced analytical paper device, incorporating the film-based sensors, that was developed could potentially respond to varying 1-HP concentrations for use in conjunction with a smartphone.

Furthermore, the developed method shows comparable selectivity between 1-HP and other components of urine. The luminance response of our sensors is not only unique but is easy to monitor by the naked eye. We consider this proof-of-concept assay to demonstrate the potential of this versatile sensor as a technique capable of discriminating between urine analytes with high structural similarity in a complex biological matrix.

2. Experimental Section

2.1 Materials and Instruments

3-thiopheneacetic acid (98%), polyethylene glycol (M_n 2000 g mol^{-1}), n-butyllithium (1.6 M in hexane), tributyltin chloride (96%), 4,7-dibromobenzo[c][1,2,5] thiadiazole (99.5%), bis(triphenylphosphine)palladium(II) dichloride, dicyclohexyl carbodiimide (DCC, 99%), 4-(*N*,*N*-dimethylamino)-pyridine (DMAP, 98%), *N*-hydroxysuccinimide (NHS, 98%), 2,5-thiophenediboronic acid (TDBA), tetrakis(triphenylphosphine) palladium(0), potassium carbonate, 1-hydroxypyrene (98%), urea, creatine, uric acid (UA), hippuric acid (HA), and glucose (Glu) were obtained from Sigma-Aldrich. (2,5-dibromo-thiophene-3-yl)-acetic acid (1) and dibromothiophene-conjugated PEG (2) were prepared in our previous work (Tawfik *et al*. 2020). All reagents were used as received.

FT/IR-6300 Fourier Transform Infrared Spectrometer (Jasco, Japan), ^{1}H NMR and ^{13}C NMR spectra (400 MHz, Bruker NMR instrument) were used for characterization of monomers and polymers. Elemental analysis was performed on vario EL elemental analyzer. The fluorescence spectra were collected using an FP-6500 spectrofluorometer (Jasco, Japan, a quartz cuvette with a 1-cm path length). The absorption spectra were collected using UV/Vis spectrophotometer (Agilent 8543, Agilent, USA). The morphological structure of the MOFs was measured using Field Emission Scanning Electron Microscope (FE-SEM, CZ/MIRA I LMH microscope). TEM measurements were

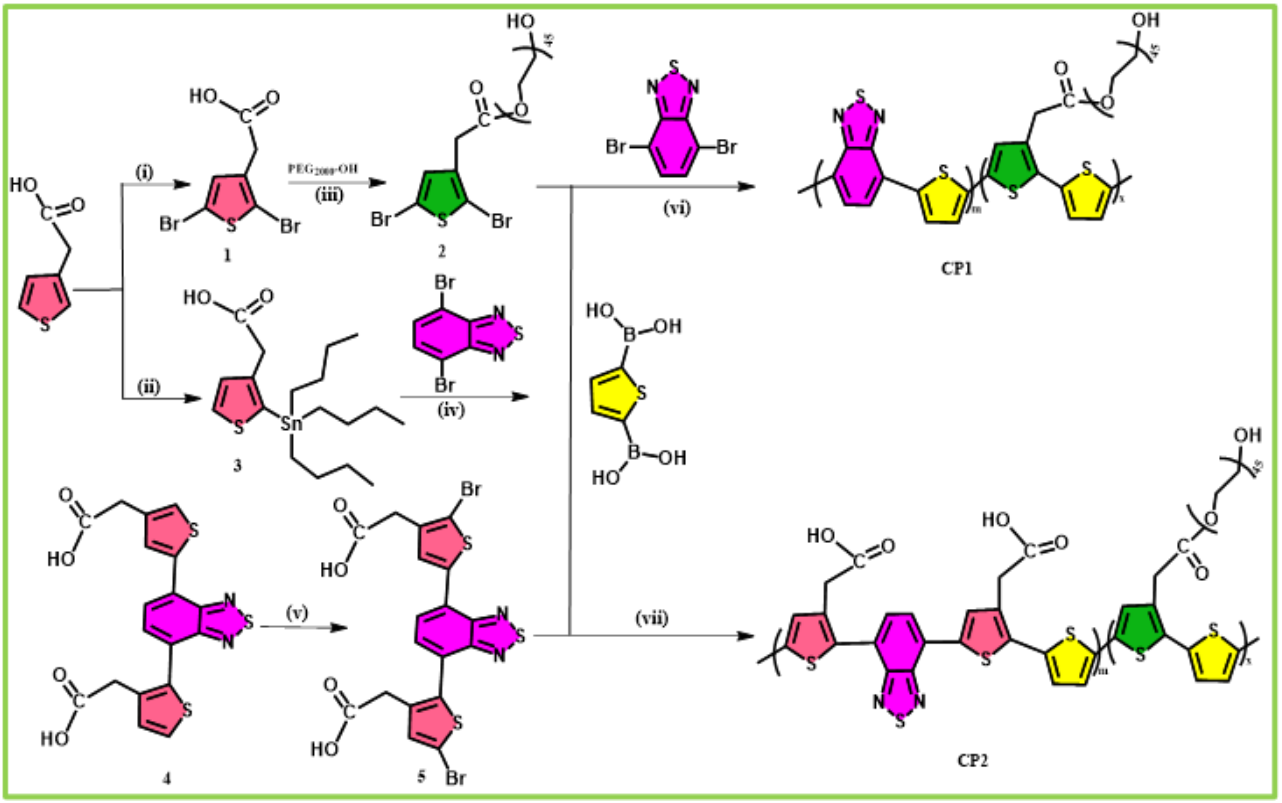

Scheme 1 Synthesis of thiophene monomers and nonionic conjugated polythiophenes: (i) NBS, dry DMF, 24 h, (ii) THF, −78 °C, n-BuLi, 2 h, (iii) DMAP, DCC, anhydrous CH_2Cl_2, 48 h, (iv) $Pd(PPh_3)_2Cl_2$, THF, 80 °C, 24 h, (v) DMF, 0 °C, NBS, 11 h, (vi, vii) THF, 2.0 M K_2CO_3, $Pd(PPh_3)_4$(0), 70 °C, 48 h.

recorded using a JEM-2100F transmission electron microscope (JEOL, 200 kV, Tokyo, Japan). The molecular weight of the prepared conjugated polythiophene ligands was determined with a Viscotek GPCmax 2001 + Viscotek TDA (RI + VISC + RALS, poly(ethylene oxide) standards). Thermo Gravimetric Analysis was carried out using (TGA, SDT Q600 V20.9 Build 20). The Brunauer-Emmett-Teller surface area (BET) of the MOFs were carried out using BET & Pore size analysis II (Autosorb-iQ). The paper sensors fabrication and the photoluminescence quantum yields determination were performed as in our reported work (Tawfik, Elmasry *et al*. 2020).

2.2 Synthesis of 2-(2-(tributylstannyl) thiophen-3-yl) acetic acid (3)

Under nitrogen atmosphere, thiophene-3-acetic acid (0.8g, 5.6 mmol) in 20 mL of THF was cooled to 78 °C. Dropwise addation of 4.2 mL (6.72 mmol) of n-BuLi (1.6 M in hexane) to the solution were performed, and the reaction mixture was stirred for 2 hours at room temperature. The solution was then cooled to 0 °C before adding 1.6 mL (5.90 mmol) of tributyltin chloride and stirring for 2 hours. The mixture was then poured into water and diluted with hexane to extract with brine. After the organic extract was separated and dried on $MgSO_4$ the solvent was evaporated under low pressure. To obtain product **3** as a yellow oil, was purified using flash column chromatography with hexane. Yield: 63%, ^{1}H NMR (400 MHz, DMSO-d_6, δ see **Fig. 1(a)**): 11.24 (s, 1H, COO**H**), 7.36 (s, 1H, thiophene), 7.17 (s, 1H, thiophene), 3.61 (s, 2H, C**H**$_2$COOH), 1.90 (m, 6H, C**H**$_2$CH$_2$CH$_3$), 1.46 (m, 6H, C**H**$_2$CH$_3$), 1.24 (t, 6H, SnC**H**$_2$CH$_2$), 0.90 (t, 9H, CH$_2$C**H**$_3$), ^{13}C NMR (400 MHz, DMSO-d_6, δ, see **Fig. 1(b)**), 173.98 (C_e), 143.59 (C_f), 135.59 (C_c), 129.04 (C_b), 127.42 (C_a), 37.12 (C_d), 29.12-12.45 (C_g- C_v), Anal. calcd for $C_{18}H_{32}O_2SSn$: C, 50.15, H, 7.47, S, 7.42, Found: C, 50.13, H, 7.49, S, 7.38.

2.3 Synthesis of 2,2'-(benzo[c][1,2,5]thiadiazole-4,7-diylbis(thiophene-5,3-diyl))diacetic acid (4)

0.115 g (0.16 mmol) of $Pd(PPh_3)_2Cl_2$ and 1.14 g (2.64 mmol) of 3 were placed in a round-bottomed two-necked flask. After degassing the flask with nitrogen, 1.82 g (6.12 mmol) of 4,7-dibromobenzo[c][1,2,5]thiadiazole in THF (35 mL) was introduced and refluxed for 24 hours at 80 °C. After that, 10 mL of hexane was injected, and the organic extract was evaporated using a rotary evaporator to prepare the sample for column chromatography purification ((CH_2Cl_2/hexane 1:5 (v/v)). Pure 1 g of the 4 was produced as an orange oil. Yield: 71%, ^{1}H NMR (400 MHz, DMSO-d_6, δ, see Fig. 1(c)): 10.33 (s, 1H, CH_2COOH), 7.86 (d, 1H, thiadiazole), 7.35 (s, 1H, thiophene), 7.10 (d, 1H, thiophene), 3.51 (s, 2H, CH_2COOH), ^{13}C NMR (400 MHz, DMSO-d_6, δ, see Fig.1(d)), 171.77 (C_e, C_u), 151.47 (C_n, C_o), 141.51 (C_f, C_p), 134.77 (C_c, C_r), 130.95-126.52 (C_g-C_q), 35.56 (C_d, C_t), Anal. calcd for $C_{18}H_{12}N_2O_4S_3$: C, 51.90, H,

2.91, N, 6.75, S, 23.11, Found: C, 51.92, H, 2.89, N, 6.74, S, 23.10.

2.4 Synthesis of 2,2'-(benzo[c][1,2,5] thiadiazole -4,7-diylbis(2-bromothiophene-5,3-diyl))diacetic acid (5)

In a round-bottomed single-necked flask, 0.787 g (1.89 mmol) of 4 was dissolved in 30 mL of DMF and cooled to 0 °C. A dropping funnel was used to add 0.7 g (3.93 mmol) of n-bromosuccinimide (10 mL of DMF) dropwise to the solution. The reaction mixture was stirred in the dark at room temperature for 11 hours, then poured into water, diluted with CH2Cl2, and extracted with brine. The organic layer was separated and dried over MgSO4, and the solvent was evaporated under low pressure. Purification of the crude product using hexane on a silica gel column yielded 1 g (76%) of 5 as a deep red solid. Yield: 76%, ^{1}H NMR (400 MHz, DMSO-d_6, δ, see Fig. 1(e)): 10.46 (s, 1H, CH_2COOH), 7.77 (d, 1H, thiadiazole), 7.26 (s, 1H, thiophene), 3.46 (s, 2H, CH_2COOH), ^{13}C NMR (400 MHz, DMSO-d_6, δ, see Fig. 1 (f)), 174.08 (C_d, C_u), 151.08 (C_o, C_n), 138.91 (C_f, C_q), 129.40-126.91 (C_g-C_p), 115.97 (C_a, C_s), 36.53 (C_c, C_t), Anal. calcd for $C_{18}H_{10}N_2O_4S_3Br_2$: C, 37.64, H, 1.77, Br, 27.84, N, 4.89, S, 16.74, Found: C, 37.61, H, 1.72, Br, 27.80, N, 4.82, S, 16.73.

2.5 Synthesis of the nonionic conjugated polythiophene ligands

According to our published work, the nonionic conjugated ligands were prepared via the Suzuki coupling approach (Tawfik, Elmasry *et al*. 2020). Monomers **1** (0.3 g, 1.0 mmol), **2** (0.23 g, 0.10 mmol), or **5** (0.342 g, 1.0 mmol) and 2,5-thiophenediboronic acid (0.206 g, 2.2 mmol) were mixed in THF (15 mL) and then 5 mL of aqueous K_2CO_3 (2.0 M) were added to a 100 mL flask. Before and after the addition of $Pd(PPh_3)_4$(0), the reaction mixture was purged with nitrogen repeatedly (27 mg, 0.023 mmol). The reaction mixture was stirred at 70 °C for 48 hours under nitrogen and then cooled to room temperature. The resultant solution was extracted with CH2Cl2, washed three times with brine and three times with DI water, dried over anhydrous sodium sulphate, and concentrated using a rotary evaporator. The solid residue was redissolved in chloroform (2 mL) and added dropwise to the methanol (50 mL). Filtration was used to collect the precipitates, which were then washed in methanol and dried in vacuum, yielding a light yellow solid CP1 and a dark yellow solid CP2. CP1: Yield: 70%, ^{1}H NMR (400 MHz, D_2O, δ, see Fig. 1(g)): 7.64 (d, 1H, thiadiazole), 7.62 (d, 1H, thiophene), 7.61 (d, 1H, thiadiazole), 7.58 (d, 1H, thiophene), 7.57 (s, 1H, thiophane), 6.71 (d, 1H, thiophane), 6.71 (d, 1H, thiophane), 5.11 (t, 1H, OH), 4.26 (t, 2H, OCH_2CH_2), 3.67 (s, 2H, thiophene-CH_2), 3.3 (q, nH, OCH_2CH_2 in PEG unit), GPC (water, poly(ethylene oxide) standard), M_n :18.321 kDa, PDI: 1.21. CP2: Yield: 68%, ^{1}H NMR (400 MHz, D_2O, δ, see Fig. 1(h)): 7.88 (d, 1H, thiadiazole), 7.77 (d, 1H, thiadiazole), 7.39 (s, 1H, thiophene), 7.21 (s, 1H, thiophene), 7.17 (d, 1H, thiophene), 7.06 (d, 1H, thiophene), 6.96 (s, 1H, thiophene), 6.86 (d, 1H, thiophane), 6.71 (d, 1H, thiophane), 4.26 (q, nH, OCH_2CH_2 in PEG unit), 3.86 (s, 2H, thiophene-CH_2), 3.44 (t, 1H, OH), GPC (water, poly(ethylene oxide) standard), M_n :25.524 kDa, PDI: 1.34.

2.6 Synthesis of CPs-Eu-MOFs

Conjugated ligands (CP1 or CP2, 0.1 mmol)) and $Eu(NO_3)_3{\cdot}6H_2O$ (0.1 mmol) were dissolved in H_2O (10 mL) in a 20 mL glass vial and placed in an oven at 90 °C for 72 h. After cooling the mixture to room temperature, a light brown solid was collected by centrifugation, and then the solid was washed several times with distilled water and methanol and dried for 24 h at 120°C under vacuum to remove the organic impurities from MOF pores. Yield: 76% based on Eu.

2.7 Procedures for 1-HP Sensing

Aqueous solution of CP1-Eu-MOF and CP2-Eu-MOF (1 mg mL^{-1}) was prepared in PBS, and then different concentrations of 1-HP (0.025, 0.25, 0.5, 5.0 and 10 nM) were added into the above solution. The luminescent spectra of the mixtures were recorded after sonication for 20 min. Moreover, the selectivity experiments for CP1-Eu-MOF and CP2-Eu-MOF were similarly carried out by adding other substance included urea, creatine, uric acid (UA), hippuric acid (HA), Na^+, K^+, NH4 +, Cl−, and glucose (Glu) (10^{-3} M) into the aqueous suspensions of CP1-Eu-MOF and CP2-Eu-MOF (1 mg mL^{-1}), and then luminescent spectra of the suspensions were recorded after being sonicated for 20 min.

For real application, human urine samples were collected and subjected to a 50-fold dilution process with a PBS solution (10 mmol L^{-1}, pH 7.4) before analysis. In a typical assay, spiked samples were prepared by adding different concentrations of 1-HP (0.1, 1.0, and 10 nM) and CP1-Eu-MOF and CP2-Eu-MOF to the diluted urine samples. The as-prepared samples were excited with 250 and 256 nm light then emission spectra were collected after 20 min, respectively. All the experiments were repeated in triplicate and performed at room temperature.

2.8 Fabrication of paper device combined with smartphone

Filter paper was coated with the CP1-Eu-MOF and CP2-Eu-MOF (0.1 mg mL^{-1}). Then, the filter paper was dried at room temperature to get the 1-HP paper-based sensors. To detect 1-HP in urine, 10 μL of diluted urine with different concentrations of 1-HP (0.005-10 nM) were dropped on the testing zone of paper sensors. The corresponding luminescence colors were then visualized under 256 nm UV light, the luminescence photos were taken by a mobile phone in a home-made box. The bright spots in the images were analyzed by the phone application (PAD Analysis), and the average intensity of red, green, and blue color was measured from the RGB channels (5 independent times). The R/B value was used to determine 1-HP concentrations using paper devices.

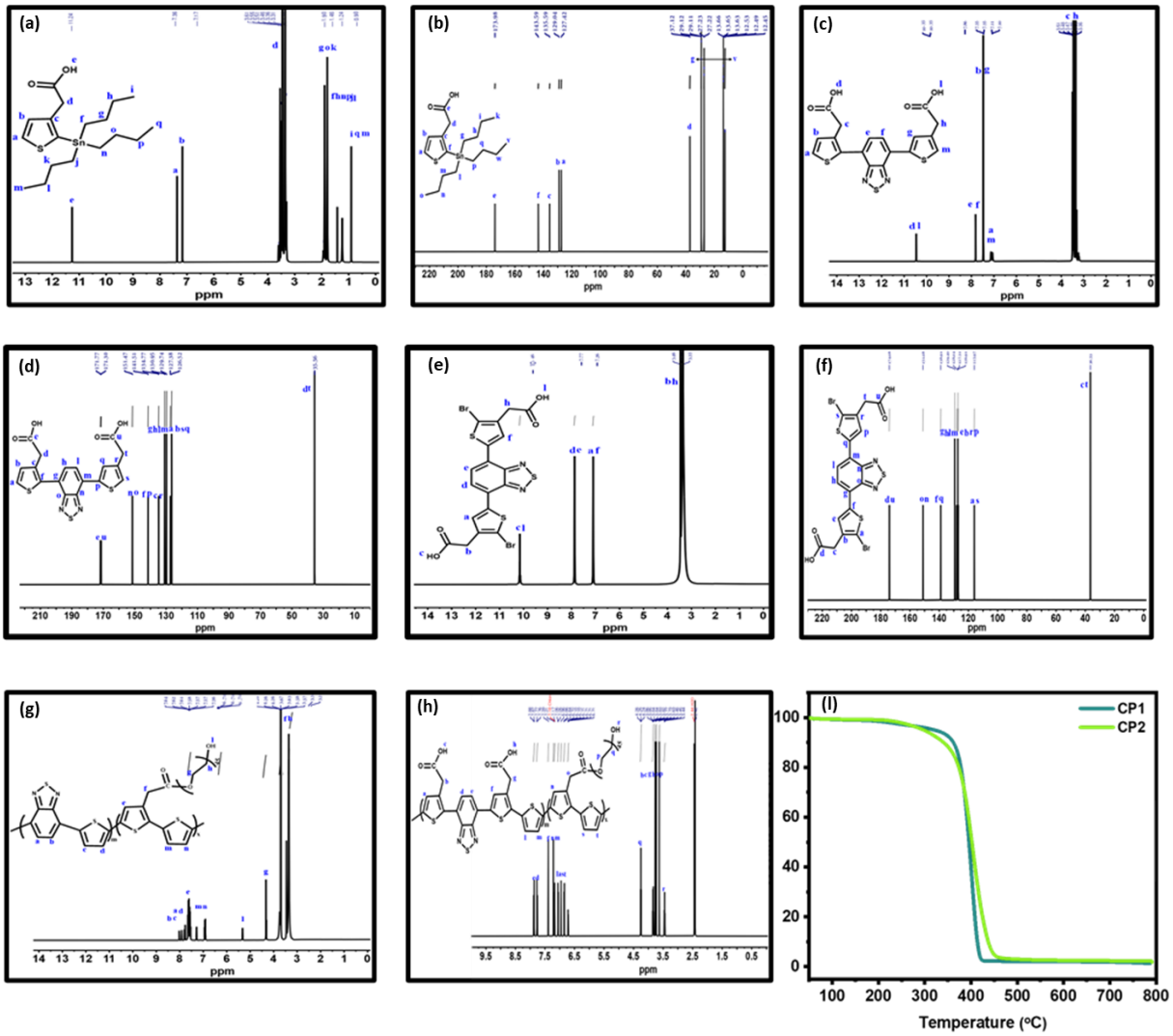

Fig. 1 (a) ^{1}H-NMR spectra of 2-(2-(tributylstannyl)thiophen-3-yl)acetic acid (3). (b) ^{13}C-NMR spectra of 2-(2-(tributylstannyl)thiophen-3-yl)acetic acid (3). (c) ^{1}H-NMR spectra of 2,2'-(benzo[c][1,2,5]thiadiazole-4,7-diylbis (thiophene-5,3-diyl))diacetic acid (4). (d) ^{13}CNMR spectra of 2,2'-(benzo[c][1,2,5]thiadiazole-4,7-diylbis(thiophene-5,3-diyl))diacetic acid (4). (e) ^{1}H-NMR spectra of 2,2'-(benzo[c][1,2,5]thiadiazole-4,7-diylbis(2-bromothiophene-5,3-diyl))diacetic acid (5). (f) ^{13}C-NMR spectra of 2,2'-(benzo[c][1,2,5]thiadiazole-4,7-diylbis(2-bromothiophene-5,3-diyl))diacetic acid (5). (g) ^{1}H-NMR spectra of nonionic conjugated polythiophene ligand, CP1. (h) ^{1}H-NMR spectra of nonionic conjugated polythiophene ligand, CP2. (l) TGA thermograms of CP1 and CP2 at a heating rate of 10°C min^{-1} from room temperature to 800°C in air.

2.9 Preparation of CP2-Eu-MOF/PVDF luminescent film

CP1-Eu-MOF powder (0.005 g) was mixed with PVDF (0.02 g) in DMF (1.25 mL). After sonication for 10 min, the mixture was drop casted onto a glass slide, pre-heated to a temperature of 140 °C in a conventional oven. Then, the solvent was allowed to evaporate at the same temperature for approximately 30 min. The resulting film was detached from the substrate, washed thoroughly with ethanol and dried at air. The film strips were immersed into aqueous solutions containing various concentration of 1-HP (0.025-10 nM) for a period of 30 min. The corresponding luminescence colors were then visualized under 256 nm UV light.

3. Results and discussion

3.1 Design, synthesis, and characterization of CP-Eu-MOFsr

Because of their biocompatibility, superior photo-stability, and high extinction coefficients, amphiphilic conjugated polythiophene nanohybrids have been widely used in environmental and biomedical sensing applications (Tawfik *et al*. 2018b, 2019, 2020, 2021, Ou *et al*. 2020, Ha Lee *et al*. 2021, Shim *et al*. 2021). In this study, we designed and synthesized two novel nonionic conjugated polythiophenes, CP1 and CP2, based on a Suzuki coupling reaction (Scheme 1). This method provided rapid access to the functionally distinct ligand that was proposed to

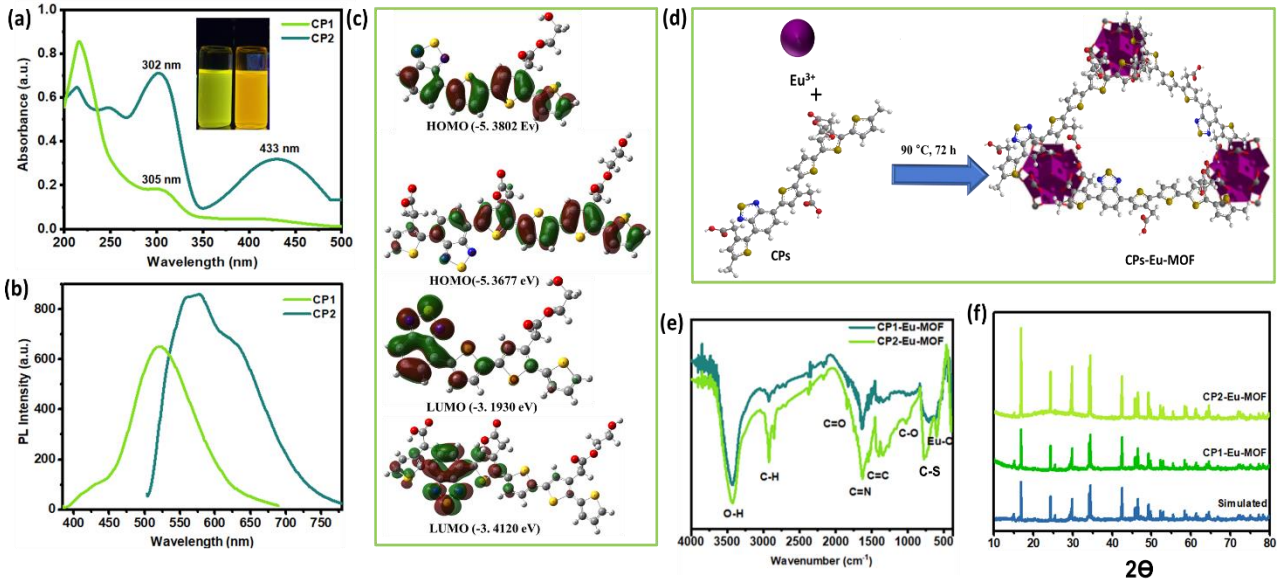

Fig. 2 (a) UV–vis absorption spectra of CP1 and CP2 ligands at a concentration of 1.0 mg/mL in DI water. Photographic image (inset) of the respective solutions (1.0 mg/ mL in DI water), illuminated by UV light. (b) PL spectra of CP1 (λ_{ex} at 305 nm) and CP2 (λ_{ex} at 433 nm). (c) Optimized geometries and molecular orbital surfaces of the HOMO and LUMO of the CP1 and CP2 ligands. (d) Synthesis of CP-Eu-MOFs. (e) FTIR spectra of CP1-Eu-MOF and CP2-Eu-MOF. (f) PXRD patterns of simulated pristine MOF, CP1-Eu-MOF, and CP2-Eu-MOF.

enhance the water solubility, biocompatibility, and sensitivity. The oxygen and nitrogen atoms as well as the tunable nature and architecture of these CPs facilitate effective coordination with Eu^{3+}. In addition, the π-conjugated system can generate an important "antenna effect" for Eu^{3+} excitation (Phaomei and Yaiphaba 2015). The detailed synthesis procedures of the two CP ligands prepared in this research are included in the ESI. The mean molecular weights (M_n) were measured using gel permeation chromatography (GPC) to be 18.32 and 25.52 kDa with and polydispersity indexes of 1.21, and 1.34 for the CP1, and CP2 ligands, respectively. The structures of CP1 and CP2 were confirmed by ^{1}H NMR spectroscopy, with the characteristic signals of the polythiophene units detected at 6.71–7.64 ppm and 6.71–7.88 ppm for CP1 and CP2, respectively. The distinctive peaks of the PEG units appeared at 3.44–5.11 ppm and 3.3–4.26 ppm for CP1 and CP2, respectively. Thermo-gravimetric analysis (TGA) was used to investigate the thermal properties of the designed CP1 and CP2 ligands. As shown in Fig. 1(l), 5% weight loss was measured at 323 and 300 °C, the decomposition temperatures of CP1 and CP2, respectively, indicating that the conjugated ligands are thermally highly stable with no phase change noticeable up to 300 °C. The optical properties of the CP1 and CP2 ligands were studied by recording their UV–vis and PL spectra in DI water, as shown in Figs. 2(a)-(b), respectively. The PL emission of CP2 is red shifted by almost 56 nm relative to that of CP1, which probably results from the more extended π-conjugated system of the dithiozolene unit that was introduced. The fluorescence of CP1 and CP2 occurred at approximately 522 and 578 nm, upon excitation at 305 and 433 nm, respectively. The photoluminescence quantum yields (PLQY) of CP1 and CP2 with reference to rhodamine B were measured to be 58 and 65% in aqueous solution, respectively.

In addition, the HOMO and LUMO energy levels of CP1 and CP2 were calculated to be −5.3802 and −3.1930 eV and −5.3677 and −3.1420 eV, respectively. The optical bandgap energies of the CP1 and CP2 ligands were also calculated to be 2.19 and 1.95 eV, Fig. 2 (c), respectively. In this detection system, the recognition toe was designed on the basis of integrating the CPs into Eu-MOF, shown in Fig. 2 (d), because of its excellent π-π and extensive hydrogen bonding interactions with 1-HP. These features are supposed to inhibit the low-frequency vibrations of Eu-MOF and promote its unique emission enhancement. In addition, the utilization of CPs as the MOF linker is expected to successfully contribute to other competitive mechanisms and to have multifunctional roles at the emission detection interface. The FTIR spectra display the main characteristic peaks of the conjugated polymers linked to Eu-MOF at υ 3425, 2922, 2859, 1739, 1640, 1460, 1019, 776, and 599 cm^{-1}, corresponding to O–H, C–H_{as}, C–H_{sy}, C=O ester, C=N, C=C, C–O, C–S, and Eu-O, Fig. 2(e). The X-ray diffraction (XRD) peaks of the prepared CP1-Eu-MOF and CP2-Eu-MOF correspond well with the simulated peaks, Fig. 2(f) confirming the phase purity of CP1-Eu-MOF and CP2-Eu-MOF. The TGA of CP1-Eu-MOF and CP2-Eu-MOF was conducted in the temperature range from 40 to 800°C, as displayed in Fig. 3(a). The CP-Eu-MOFs underwent 5% weight loss during decomposition in the temperature range 40-322°C (CP1-Eu-MOF) and 40-397°C (CP2-Eu-MOF), respectively, which is attributed to the elimination of water molecules from the pores. Further heating resulted in a sudden and pronounced weight loss due to the decomposition of the framework. Ligand degradation of the conjugated polymers occurs at higher

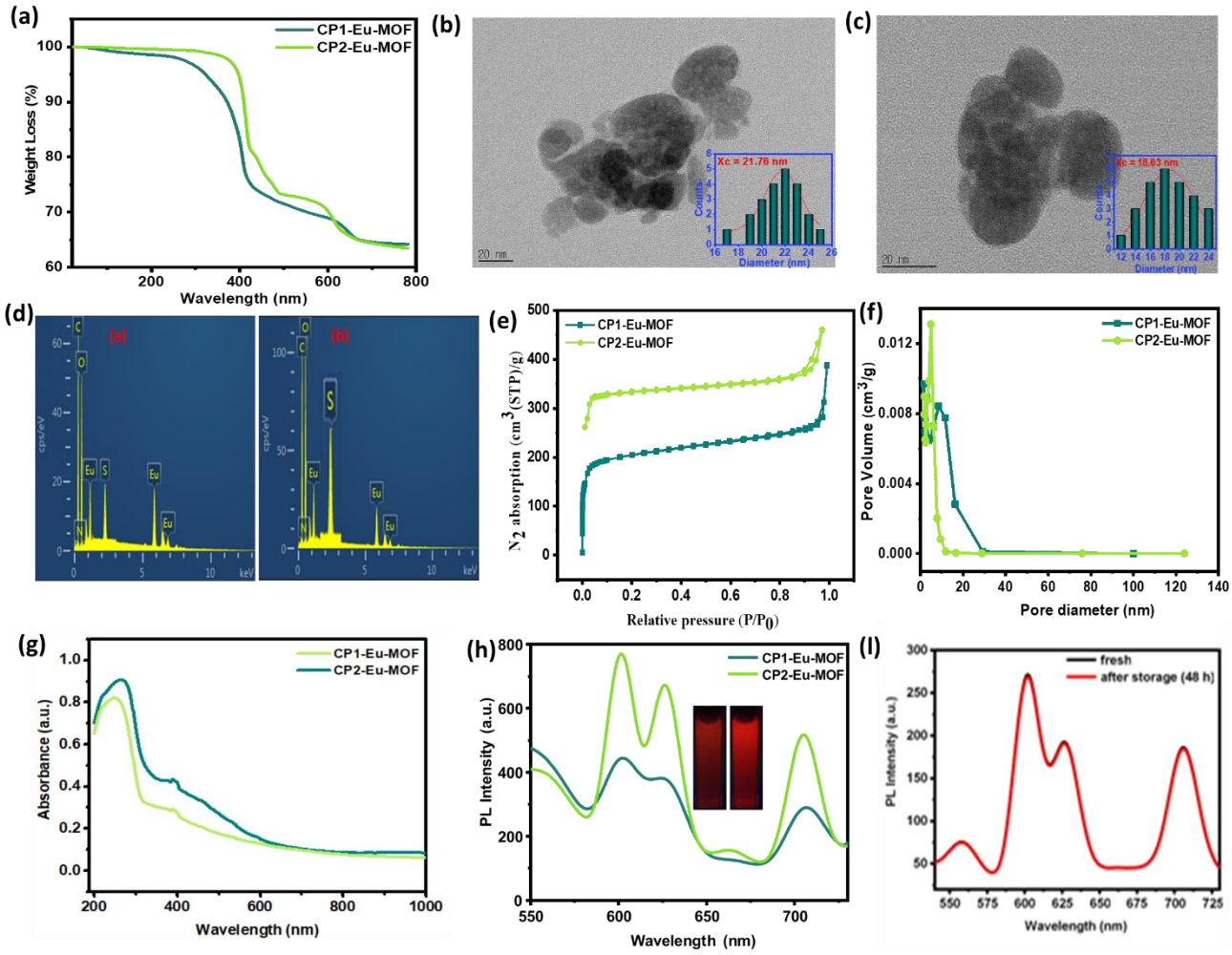

Fig. 3 (a) TGA thermograms of CP1-Eu-MOF and CP2-Eu-MOF recorded at a heating rate of 10°C min-1 from room temperature to 800°C in air. (b, c) TEM images and histograms representing the diameter of CP1-Eu-MOF, and CP2-Eu-MOF. (d) EDX spectra of the designed CP1-Eu-MOF and CP2-Eu-MOF. (e) N_2 adsorption-desorption isotherms of CP1-Eu-MOF and CP2-Eu-MOF samples. (f) Pore size determination of CP1-Eu-MOF and CP2-Eu-MOF samples. (g) Excitation of CP1-Eu-MOF and CP2-Eu-MOF. (h) Emission spectra of CP1-Eu-MOF and CP2-Eu-MOF. Inset: corresponding photographic images of the solutions under irradiation with 254 nm UV-light. (l) Luminescent spectra of CP1-Eu-MOF before (black) and after (red) storage in water for 48 h

temperatures (between 423 and 666 °C) because the Eu ions and polythiophene ligands are strongly connected through Eu−O−C bonds. The morphological features and size distribution of the prepared MOFs indicated that the particle size of the as-synthesized CP1-Eu-MOF and CP2-Eu-MOF is in the nanoscale range (18–22 nm) and that the particles are irregularly shaped nanoplates, Figs. 3 (b)-(c). The energy-dispersive X-ray spectrometry (EDS) results clearly reveal the coexistence of the elements Eu and C, O, N, and S, Fig. 3 (d). The N_2 adsorption–desorption isotherms were recorded at 77 K to investigate the porosities of CP1-Eu-MOF and CP2-Eu-MOF. All the isotherms are type-I sorption isotherms, demonstrating the micropore characteristics of the CP-Eu-MOFs. The Brunauer-Emmett-Teller (BET) surface areas were determined to be 1100 and 1520 $m^2\ g^{-1}$ with a pore size of 8.36 and 4.88 nm for CP1-Eu-MOF and CP2-Eu-MOF, respectively, Figs. 3 (e)-(f).

3.2 Luminescence study and sensing capabilities of 1-HP

The luminescence characteristics of CP1-Eu-MOF and CP2-Eu-MOF were measured after their successful preparation. The absorption spectra of CP1-Eu-MOF and CP2-Eu-MOF consist of a wide band with the main peaks at 250 nm and 256 nm, Fig. 3(g), respectively. The CP1-Eu-MOF and CP2-Eu-MOF exhibit characteristic sharp emissions at 603, 626, 663, and 703 nm, which correspond to the Eu^{3+} transitions, $^5D_0 \rightarrow {}^7F_J$ (J = 1, 2, 3, 4), respectively, Fig. 3(h). These findings suggest that the energy absorbed by the conjugated MOFs has effectively transferred to the Eu^{3+}excition levels to sensitize the luminescence of Eu^{3+} emitters. As a result, CP1-Eu-MOF and CP2-Eu-MOF have an impressive red appearance under UV light, which is probably due to the $^5D_0 \rightarrow {}^7F_2$ transition

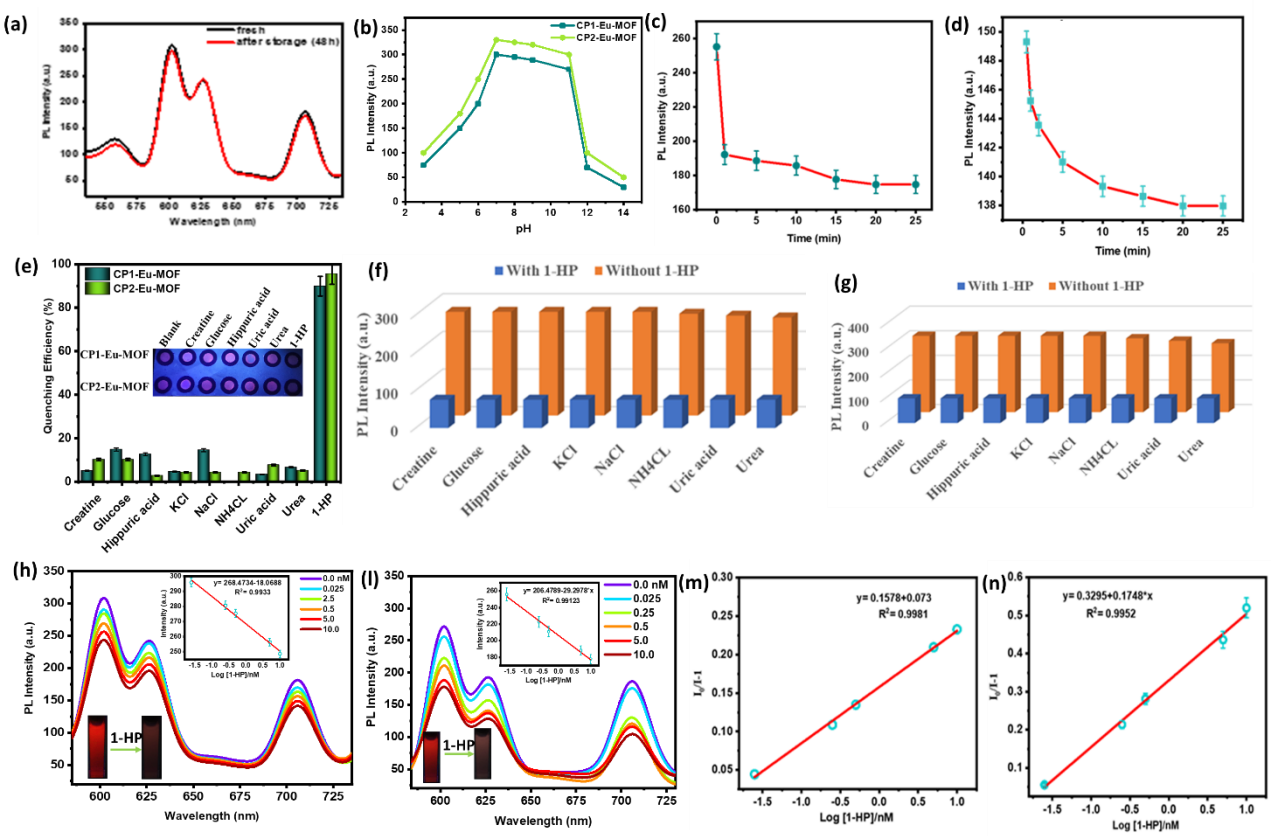

Fig. 4 (a) Luminescent spectra of CP2-Eu-MOF before (black) and after (red) storage in water for 48 h. (b) The emission intensities of CP1-Eu-MOF and CP2-Eu-MOF in aqueous solutions with different pH values (3-14). (c, d) Emission intensity at 603 nm CP1-Eu-MOF and CP2-Eu-MOF suspensions upon exposure to 1-HP at various time intervals (λ_{ex} = 250 and 256 nm, respectively). (e) Luminescence responses of CP1-Eu-MOF and CP2-Eu-MOF toward 1-HP in the presence of background of other various urine components. (f, g) Quenching efficiency of suspensions of CP1-Eu-MOF and CP2-Eu-MOF with various urine components. Inset: photographic image of the corresponding paper sensor exposed to UV light (254 nm). (h, l) Detection performance of CP1-Eu-MOF and CP2-Eu-MOF in PBS solutions (10 mmol L^{-1}, pH 7.4) containing various concentrations of 1-HP (0–10 nM). Insets: Intensity vs. 1-HP concentration and the color of the sensor solutions in PBS before and after adding 1-HP (UV irradiation at 256 nm). (m, n) S-V plots of CP1-Eu-MOF, and CP2-Eu-MOF.

of Eu^{3+} at 603 nm, Fig. 3(h) (inset). The excellent optical performance of the CP-Eu-MOFs offers favorable conditions for the detection of the desired target. The stability of the CP1-Eu-MOF and CP2-Eu-MOF sensors in aqueous medium was first investigated before assessing their feasibility for 1-HP detection. Fig. 3(l) and Fig. 4(a). show that CP1-Eu-MOF and CP2-Eu-MOF undergo no obvious changes in their luminescence intensity during two days' immersion time, demonstrating the excellent optical stability of the MOFs in aqueous medium. The effects of pH on the luminescence properties were also analyzed across a wide pH range (3.0–14.0), Fig. 4(b). Fig. 4(b) shows insignificant fluorescence change in this pH range, indicating that the prepared CP1-Eu-MOF and CP2-Eu-MOF are suitable for use in aqueous and biological media. This unprecedented aqueous stability of the CP-Eu-MOFs is probably owing to the strong coordination bonds (Eu-O), which assist the MOFs to survive against attacks and hydrolysis with the water molecules. Additionally, the luminescent response with respect to the incubation time of CP1-Eu-MOF and CP2-Eu-MOF towards 1-HP is quite rapid, as shown in Figs. 4(c)-(d). The luminescence of CP1-Eu-MOF and CP2-Eu-MOF noticeably decreases at once after the addition of 1-HP. After an extended incubation period (20 min) the decline in emission stabilizes to reach a constant level. Therefore, the results suggest that the established strategy for the recognition of 1-HP by CP1-Eu-MOF and CP2-Eu-MOF is appropriate.

High sensitivity and excellent selectivity of a sensor to the detecting targets are highly desired for practical applications. Thus, an experiment to determine the selectivity of CP1-Eu-MOF and CP2-Eu-MOF toward other common components of urine, such as creatine, glucose, hippuric acid, K^+, Na^+, NH_4^+, uric acid, and urea was carried out. As presented in Fig. 4(e), the changes in the emission of CP1-Eu-MOF or CP2-Eu-MOF are found to be nonsignificant when the sensors are exposed to urine components other than 1-HP. A wax-printed paper sensor was also utilized to emphasize the selectivity and showed that only 1-HP induces a significant change in the luminescence intensities of CP1-Eu-MOF and CP2-Eu-MOF upon exposure to UV light. This difference is

Table 1 Comparison of this work with the reported methods for the assay of 1-HP

Materials	Detection technique	Linear range	LOD	Ref.
Polystyrene/oxidized carbon nanotubes film	mass spectrometry	2.29 – 91.64 nM	–	(He, Zhu *et al.* 2014)
diethoxydiphenylsilane fibre	gas chromatography	0.458–9.16 nM	–	(Mattarozzi, Musci *et al.* 2009)
molecularly imprinted polymer	HPLC-FLD	0.687–9.16 nM	0.229 nM	(Serrano, Bartolome *et al.* 2015)
molecularly imprinted polymer	solid phase extraction	45.8 nM–1.83 μM	14.2 nM	(Serrano, Bartolomé *et al.* 2017)
hydroxyl-propyl beta-cyclodextrin	synchronous fluorimetry	20 nM–12μM	4.2 nM	(Zhang, Zhu *et al.* 2015)
Graphene oxide nanoribbon	Electrochemical	0.1 –12.55 μM	40 nM	(Shen, Cui *et al.* 2012)
MIP receptors	cyclic voltammetry	1 nM – 200 nM	0.33 nM	(Yang, Lee *et al.* 2017)
PRT-AuNCs	Fluorescence	0.986 – 64.6 nM	0.296 nM	(Xue, Liu *et al.* 2019)
Conjugated Polyelectrolyte/Graphene Multilayer Films	Electrochemical	20−130 nM	10.42 nM	(Pang, Huang *et al.* 2019)
Eu-functionalized metal-organic framework	luminescence	0 to 1.0 mg L^{-1}	0.69 μg L^{-1}	(Hao and Yan 2017)
Conjugated polymer self-assembled with graphene	Electrochemical	0.5 to 120 nM	0.07 nM	(Pang, Yang *et al.* 2020)
Nonionic Conjugated Polythiophenes-Functionalized Eu-MOF	luminescence	0.025 to 10 nM 0.025 to 10 nM	1.66 pM 1.02 pM	this work

Table 2 Determination of 1-HP in real human urine samples by the proposed sensors

Sensors	Spiked (nM)	Found* (nM)	Recovery (%)	RSD (%)
	0.00	0.00	------	------
CP1-Eu-MOF	0.10	0.102±5.363	102.0	4.32
	1.00	0.941±4.568	94.1	3.68
	10.0	10.35±1.974	103.5	1.59
CP2-Eu-MOF	0.10	0.097±5.090	97.0	4.10
	1.00	0.999±3.029	99.9	2.44
	10.0	10.11±3.997	101.1	3.22

*The 95 % confidence interval was calculated with Student's t = 2.776 (n = 5).

differentiable with the naked eyes (see insets in Fig. 4(e)). This implies that the developed MOFs can function as visual optical sensors for 1-HP recognition. Interference experiments were also conducted to explore the potential of using CP1-Eu-MOF and CP2-Eu-MOF for 1-HP determination, by testing the luminescent responses to 1-HP in the presence of other components. Figs. 4(f)-(g) show that the emission intensity of 1-HP at 603 nm did not decline against the background of other urine components, revealing the strong anti-interference potential of CP1-Eu-MOF and CP2-Eu-MOF. These results indicate that CP1-Eu-MOF and CP2-Eu-MOF would have outstanding selectivity as sensors for 1-HP detection in real urine samples without interference by other urine components.

The high stability and the outstanding luminescent properties of CP1-Eu-MOF and CP2-Eu-MOF inspired us to investigate their molecular recognition ability by engaging in hydrogen bonding and π−π interactions. To be eligible CP1-Eu-MOF and CP2-Eu-MOF sensors for 1-HP urinary biomarker detection, water tolerance is a necessity for CP1-Eu-MOF and CP2-Eu-MOF because 1-HP is dispersed in an aqueous medium. As a demonstration of this concept, the detection responses of 1-HP were investigated by introducing 1-HP into suspensions of CP1-Eu-MOF and CP2-Eu-MOF and analyzing their luminescence intensity. As displayed in Figs. 4(h)-(l), an apparent decline in the luminescence intensity of Eu^{3+} at 603 nm was observed by adding different concentrations of 1-HP ranging from 0.025 to 10 nM to suspensions of CP1-Eu-MOF and CP2-Eu-MOF. The limit of detection (LOD) was determined to be 1.66 pM for CP1-Eu-MOF and 1.02 pM for CP2-Eu-MOF using $3\sigma/s$ (Tawfik *et al.* 2018a), where σ is the standard deviation of blank intensities for twenty measurements and *s* is the slope of the obtained linear curve (insets in Figs. 4(h)-(l), respectively. These LODs are much lower than those of many of the state-of-the-art 1-HP sensors (Table 1)

and the benchmark value for 1-HP in urine (1.0 μg/L) according to the recommendation of the American Conference of Governmental Industrial Hygienists (Jongeneelen 2014). This result would be able to meet the daily requirements for the biomonitoring of PAHs and also demonstrates the exceptional sensitivity of CP1-Eu-MOF and CP2-Eu-MOF sensors towards 1-HP. In addition, the sensors can be observed visually to undergo quenching when exposed to 256 nm UV light, here the color of the sensors is visibly darkened as soon as 1-HP is introduced (inset of Figs. 4(h)-(l). The luminescence quenching efficiency can be quantitatively explained by the linear Stern–Volmer (S–V) equation:

$$I_0/I=K_{SV}[C]+1 \quad (1)$$

where I_0 and I are the emission intensities before and after 1-HP addition, K_{sv} is the quenching constant (M^{-1}), and [C] is the molar concentration of the 1-HP, respectively (Tawfik *et al*. 2018a). For CP1-Eu-MOF, the linear relationship can be presented by $I_0/I-1 = 0.1578+0.073$ [C], with $R^2 = 0.9981$, whereas, the linear correlation for CP2-Eu-MOF can be expressed by $I_0/I-1 = 0.3295 + 0.1748$ [C], with $R^2 = 0.9952$ (see Figs. 4 (m)-(n)). The K_{sv} values for 1-HP were calculated to be 73×10^6 M^{-1} and 174×10^6 M^{-1} in the presence of CP1-Eu-MOF and CP2-Eu-MOF, respectively. This finding suggests that CP1-Eu-MOF and CP2-Eu-MOF are excellent luminescent sensors for 1-HP analysis over a wide range of concentrations.

Recyclability is a highly important matter when assessing the feasibility of a sensing material. Consequently, the recycling efficiency of CP1-Eu-MOF and CP2-Eu-MOF was also investigated, Figs. 5(a) and 5(b). After sensing experiments with CP1-Eu-MOF and CP2-Eu-MOF, each of the sensing materials with 1-HP was collected using centrifugation and rinsed three times with water using sonication. The findings indicate that the intensities of CP1-Eu-MOF and CP2-Eu-MOF can be restored through centrifugation of the suspension. Figs. 5(a) and 5(b) show that both the emission and the quenching performance of the recycled sensors remain approximately the same as those of the initial sensors after five cycles. Meanwhile, the PXRD patterns of the recycled CP1-Eu-MOF and CP2-Eu-MOF indicate that their crystals are stable after five cycles, Figs. 5(c) and 5(d). These findings reveal the superior reusability of the sensors and indicate that the framework structure remained intact, and the emission did not decline. The results highlight the potential for using CP1-Eu-MOF and CP2-Eu-MOF in practical applications.

To assess the practical performance of the constructed sensors for the detection of 1-HP in real applications, spiked urine samples with three different concentrations of 1-HP were analyzed by CP1-Eu-MOF and CP2-Eu-MOF. The results are summarized in Table 2, which indicates the amounts of 1-HP detected by the developed sensors with satisfactory recoveries of 94.1–103.5%. Each of the analyses of the spiked urine samples by these sensors was repeated five times and the relative standard deviations (RSDs) were determined to be less than 5%. The successful recoveries and the acceptable RSDs suggest that the developed strategy is feasible for the reliable and accurate analysis of 1-HP in a biological matrix.

3.3 Visual detection of 1-HP using luminescent paper and a sensor based on PVDF film

To develop a simple and portable sensor, 1-HP paper-based sensors were fabricated by coating wax-printed paper with CP1-Eu-MOF and CP2-Eu-MOF (0.5 mg/mL). For visual detection purposes, different concentrations of 1-HP (0.05–10 nM) were dropped onto the coated paper, which was allowed to dry at room temperature. The color of the CP1-Eu-MOF and CP2-Eu-MOF paper sensors was quenched by the addition of 1-HP and could be visualized by irradiation with 256 nm UV light. Motivated by the considerable color changes on the paper that indicate the various concentrations of 1-HP in urine, a smartphone was utilized for color image analysis using the "PAD Analysis" application for RGB determination, Fig. 5(e) (Tawfik *et al*. 2019, 2020, Ou *et al*. 2020). Using the B/R ratio and the various Log [1-HP], fitted curves were constructed that can be represented by the following equations: $y = 0.785x + 1.064$ ($R^2 = 0.9912$), $y = 0.892x + 1.2731$($R^2 = 0.9903$) with LODs of 38.21 pM and 33.63 pM for CP1-Eu-MOF and CP2-Eu-MOF, respectively, Figs. 5(f)-(g). These results revealed that on-site detection using a paper sensor is highly sensitive and promising, with this strategy only demanding a handheld UV lamp and smartphone.

A luminescent film was also fabricated using the drop-casting approach, which entailed dropping a homogeneous suspension of CP2-Eu-MOF nanoparticles and PVDF polymer onto a DMF solution on a glass slide. The spread homogeneous suspension was then dried in a pre-heated oven at 140 ºC for 30 min to form composite films, Fig. 5(h). The optimal CP2-Eu-MOF loading of these films was determined to be 50 wt% to produce robust and flexible films as shown in Fig. 5(l), whereas a larger or smaller amount of CP2-Eu-MOF resulted in weak and cracked films. The filmstrips were immersed in aqueous solutions containing various concentrations of 1-HP (0.025–10 nM) for a period of 30 min.

As displayed in Fig. 5(h), the luminescent colors of the fabricated films changed from bright light red to dark brown, and finally to dark blue with increasing 1-HP concentration. The change in the color of the film sensor can be easily differentiated by the naked eyes, with approximately 0.025 nM of 1-HP readily distinguishable by the naked eye, i.e., the naked-eye detection limit was as low as 0.025 nM (25 pM). Importantly, utilizing color changes on the films with the various concentrations of 1-HP, a smartphone was employed for color image analysis using the "PAD Analysis" application for RGB determination (see Fig. 6(h). Using the B/R ratio and the various Log [1-HP], fitted curves were constructed that can be represented by the following equations: $y = 2.387x + 1.0778$ ($R^2 = 0.9940$) with LODs of 12.5 pM for CP2-Eu-MOF/PVDF film. Therefore, this luminescent film could be successfully used for the sensitive and visual detection of 1-HP.

The recycling efficiency of the CP2-Eu-MOF/PVDF film is a very important aspect of practical application. The film was alternately exposed to 1-HP aqueous solution, and the corresponding fluorescence emission was measured. Each of the sensing films was rinsed three times with water

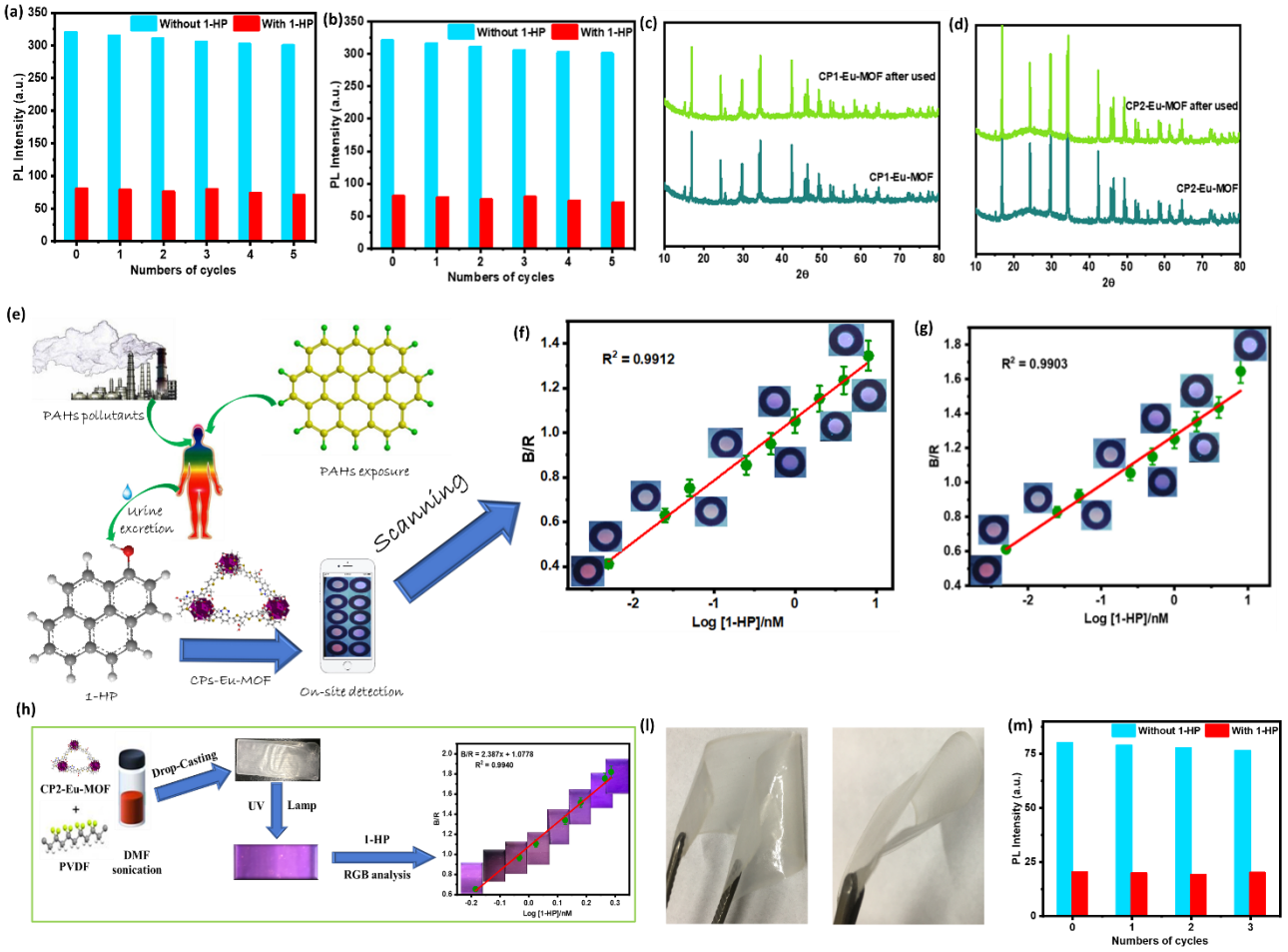

Fig. 5 (a, b) Luminescence intensities of CP1-Eu-MOF and CP2-Eu-MOF and at 603 nm during five consecutive quenching and regenerating cycles. (c,d) The XRD patterns of CP1-Eu-MOF and CP2-Eu-MOF after using five recycles. (e) Schematic diagram of the turn-of luminescence switch for on-site detection of urinary 1-HP via the fabrication of wax-printed paper sensors. (f, g) Colorimetric analysis and calibration plots of 1-HP concentration based on RGB values of the luminescence paper-based sensors in combination with a smartphone application using CP1-Eu-MOF and CP2-Eu-MOF, respectively. Error bars represent ±SD for 5 measurements. (h) Fabrication of CP2-Eu-MOF-doped transparent PVDF film in daylight, and visualization of CP2-Eu-MOF-doped PVDF luminescence film under UV light after immersion in urine spiked with different concentrations of 1-HP (lamp excitation at 256 nm) as well as the calibration plot of 1-HP concentration based on RGB values of the luminescence film-based sensors in combination with a smartphone application. (l) The fabricated CP2-Eu-MOF film images with flexible nature in bright field (MOF loading in this film was 50 wt%). (m) Luminescence intensities of CP2-Eu-MOF/PVDF film at 603 nm during three consecutive quenching and regenerating cycles.

and ethanol under sonication to assure complete removal of 1-HP from the film surface. The experiment showed that the emission of the film could be restored, as shown in Fig. 5(m). The reason for the reusability is that CP2-Eu-MOF/PVDF has a stronger complexation capability with 1-HP. This regeneration ability indicated that the CP2-Eu-MOF/PVDF film could be reused with proper treatment.

3.4 Mechanism of 1-HP Sensing

The luminescent quenching mechanism was studied in detail to improve our understanding of the nature of the interaction between the developed sensors and 1-HP. In this work, 1-HP can induce the luminescence quenching of CP1-Eu-MOF and CP2-Eu-MOF in the following three ways: (1) framework collapse via the direct interaction between the emission centers Eu^{3+} and 1-HP, (2) a FRET or photoinduced electron transfer (PET) mechanism, and (3) molecular interactions (i.e., π–π stacking, hydrogen bonding, and/or O–H···π interactions). As displayed in Figs. 5(c) and 5(d), the MOFs treated with 1-HP have the same XRD peaks as the untreated MOFs, demonstrating that the crystal structure remains unchanged after the addition of 1-HP. Typically, the quenching process probably occurs via either a FRET or PET mechanism. One important prerequisite for promoting the existence of the FRET process is that the absorption spectrum of the 1-HP (acceptor) must overlap with the emission spectrum of the conjugated polymer ligands (donor).

To confirm the high selectivity of CP1-Eu-MOF and

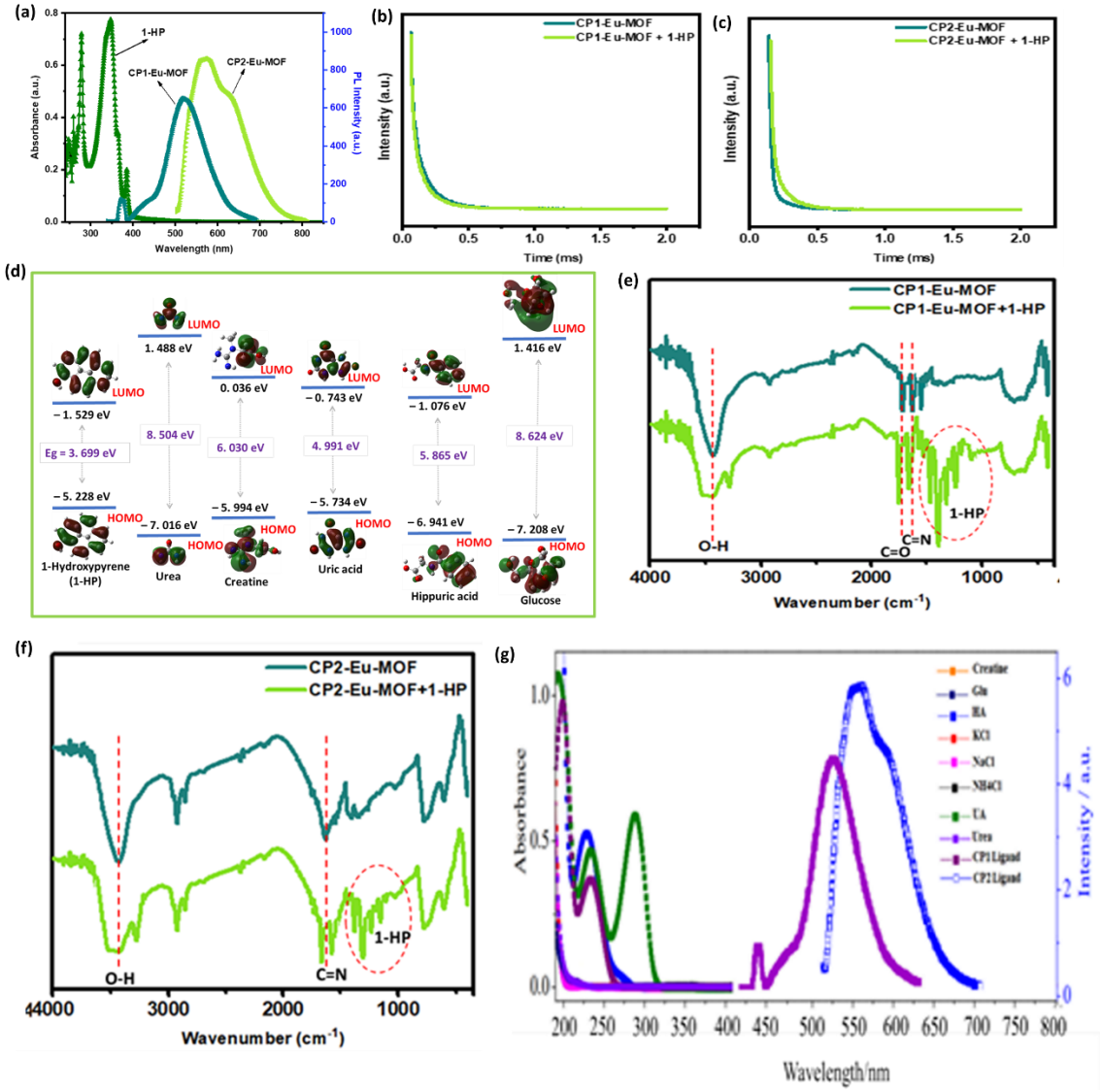

Fig. 6 (a) UV-vis spectrum of 1-HP and emission spectra of CP1-Eu-MOF and CP2-Eu-MOF. (b, c) Decay curves of CP1-Eu-MOF and CP2-Eu-MOF suspension in the absence and presence of 1-HP. (d) HOMO-LUMO energy levels of 1-HP and other analytes.(e, f) FTIR spectra of CP1-Eu-MOF and CP1-Eu-MOF+1-HP, CP2-Eu-MOF and CP2-Eu-MOF+1-HP. (g) The UV-Vis spectra of various urine components and the emission spectrum of CP1 and CP2 ligands.

CP2-Eu-MOF for the 1-HP urinary biomarker, the UV-vis spectra of the other common species in urine were recorded. As displayed in Fig. 6(g), the emission spectra of the other common urine species and the conjugated ligands do not overlap, suggesting that the FRET mechanism cannot be responsible for the interaction between the MOF ligands and urine components. Thus, the other species that are commonly found in urine have almost no effect on the luminescence of CP1-Eu-MOF and CP2-Eu-MOF, consequently, 1-HP is exclusively detected by CP1-Eu-MOF and CP2-Eu-MOF.

4. Conclusions

In summary, sensors based on nonionic conjugated Eu-MOFs were successfully developed by integrating CPs as the recognition toe and Eu3+ as the signal readout element in one MOF system for the first time,

• These sensors exhibited highly sensitive and selective detection performance toward 1-HP. Strong quenching performance, a good linear relationship between the emission intensities and the 1-HP concentrations, rapid response, and high selectivity, as well as good reusability, indicated that CP1-Eu-MOF and CP2-Eu-MOF are promising sensors for 1-HP.

• The LODs were determined to be 1.66 and 1.02 pM using CP1-Eu-MOF and CP2-Eu-MOF, respectively, which is remarkably low.

• The quenching process can be explained in terms of the molecular interaction and static quenching mechanisms.

• Furthermore, a facile assay for analyzing people's degree of exposure to PAHs was developed by designing a portable paper sensor coupled with a smartphone for on-site

detection.

• More importantly, a luminescent PVDF film doped with CP2-Eu-MOF for 1-HP detection with the naked eyes was successfully fabricated.

• The proposed strategy offers sensitive and reliable detection of 1-HP and is expected to open a new pathway for the advancement of easy-to-use diagnostic techniques to prevent environmental contamination and PAH-related diseases.

Acknowledgements

S. M. Tawfik gratefully acknowledges support from the Egyptian Petroleum Research Institute.

Funding

This work was supported by the National Research Foundation of Korea (NRF) grant funded by the Korean government (MSIT) (No. 2020R1A2C2007028).

References

Abdel-Shafy, H.I. and Mansour, M.S.M. (2016), "A review on polycyclic aromatic hydrocarbons: Source, environmental impact, effect on human health and remediation", *Egyptian J. Petrol*., **25**(1), 107-123. https://doi.org/10.1016/j.ejpe.2015.03.011.

Alekseenko, A.N., Zhurba, O.M., Merinov, A.V. and Shayakhmetov, S.F. (2020), "Determination of 1-hydroxypyrene as a biomarker for the effects of polycyclic aromatic hydrocarbons in urine by chromatography–mass spectrometry", *J. Anal. Chem*., **75**(1), 84-89. https://doi.org/10.1134/S1061934820010025.

Ankamwar, B. and Sur, U.K.J. (2020), "Copper micro/ nanostructures as effective SERS active substrates for pathogen detection", *Adv. Nano Res*., **9**(2), 113-122. http://doi.org/10.12989/anr.2020.9.2.113.

Bansal, V. and Kim, K.H.J.E.I. (2015), "Review of PAH contamination in food products and their health hazards", *Environ. Int.*, **84**, 26-38. https://doi.org/10.1016/j.envint.2015.06.016.

Castro-Grijalba, A., Montes-García, V., Cordero-Ferradás, M.J., Coronado, E., Pérez-Juste, J. and Pastoriza-Santos, I. (2020), "SERS-based molecularly imprinted plasmonic sensor for highly sensitive PAH detection", *ACS Sensors*, **5**(3), 693-702. https://doi.org/10.1021/acssensors.9b01882.

Chen, L., Ye, J.W., Wang, H.P., Pan, M., Yin, S.Y., Wei, Z.W., Zhang, L.Y., Wu, K., Fan, Y.N. and Su, C.Y.J.N.C. (2017), "Ultrafast water sensing and thermal imaging by a metal-organic framework with switchable luminescence", *Nat. Commun*., **8**(1), 15985. https://doi.org/10.1038/ncomms15985.

Cui, Y., Song, R., Yu, J., Liu, M., Wang, Z., Wu, C., Yang, Y., Wang, Z., Chen, B. and Qian, G.J.A.M. (2015), "Dual-emitting MOF⊃ dye composite for ratiometric temperature sensing", *Adv. Mater.*, **27**(8), 1420-1425. https://doi.org/10.1002/adma.201404700.

Gao, P., da Silva, E.B., Townsend, T., Liu, X. and Ma, L.Q. (2019), "Emerging PAHs in urban soils: Concentrations, bioaccessibility, and spatial distribution", *Sci. Total Environ*. **670**, 800-805. https://doi.org/10.1016/j.scitotenv.2019.03.247.

Gill, B., Jobst, K. and Britz-McKibbin, P. (2020), "Rapid screening of urinary 1-hydroxypyrene glucuronide by multisegment injection–capillary electrophoresis–tandem mass spectrometry: A high-throughput method for biomonitoring of recent smoke exposures", *Anal. Chem*., **92**(19), 13558-13564. http://doi.org/10.1021/acs.analchem.0c03212

Lee, S.H., Tawfik, S.M., Thangadurai, D.T. and Lee, Y.I. (2021), "Highly sensitive and selective detection of Alprenolol using upconversion nanoparticles functionalized with amphiphilic conjugated polythiophene", *Microchem. J*., **164**, 106010. https://doi.org/10.1016/j.microc.2021.106010.

Habibullah-Al-Mamun, M., Ahmed, M.K. and Masunaga, S.J.A.i.e.r. (2018), "Polycyclic aromatic hydrocarbons (PAHs) in surface water from the coastal area of Bangladesh", *Adv. Environ. Res.*, **7**(3), 177-200. http://doi.org/10.12989/aer.2019.7.3.177**.**

Haldar, R., Heinke, L. and Wöll, C. (2020), "Advanced photoresponsive materials using the metal–organic framework approach", *Adv. Mater*., **32**(20), 1905227. http://doi.org/10.1002/adma.201905227.

Hao, J.N. and Yan, B. (2017), "Determination of urinary 1-hydroxypyrene for biomonitoring of human exposure to polycyclic aromatic hydrocarbons carcinogens by a lanthanide-functionalized metal-organic framework sensor", *Adv. Funct. Mater*., **27**(6), 1603856. http://doi.org/10.1002/adfm.201603856.

He, X.M., Zhu, G.T., Yin, J., Zhao, Q., Yuan, B.F. and Feng, Y.Q.J.J.O.C.A. (2014), "Electrospun polystyrene/oxidized carbon nanotubes film as both sorbent for thin film microextraction and matrix for matrix-assisted laser desorption/ionization time-of-flight mass spectrometry", *J. Chromatogr. A*, **1351**, 29-36.

Hu, Z., Deibert, B.J. and Li, J.J.C.S.R. (2014), "Luminescent metal–organic frameworks for chemical sensing and explosive detection", *Chem. Soc. Rev.* **43**(16), 5815-5840. https://doi.org/10.1039/C4CS00010B.

Hu, Y., Du, C., Li, Y., Fan, L. and Li, X. (2015), "A gold nanoparticle-based colorimetric probe for rapid detection of 1-hydroxypyrene in urine", *Analyst*, **140**(13), 4662-4667. http://doi.org/10.1039/C5AN00722D.

Huang, R.W., Wei, Y.S., Dong, X.Y., Wu, X.H., Du, C.X., Zang, S.Q. and Mak, T.C.W. (2017), "Hypersensitive dual-function luminescence switching of a silver-chalcogenolate cluster-based metal–organic framework", *Nat. Chem*., **9**(7), 689-697. https://doi.org/10.1038/nchem.2718.

Jin, R., Bu, D., Liu, G., Zheng, M., Lammel, G., Fu, J., Yang, L., Li, C., Habib, A., Yang, Y. and Liu, X. (2020), "New classes of organic pollutants in the remote continental environment – Chlorinated and brominated polycyclic aromatic hydrocarbons on the Tibetan Plateau", *Environ. Int*., **137**, 105574. https://doi.org/10.1016/j.envint.2020.105574.

Jongeneelen, F.J. (2014), "A guidance value of 1-hydroxypyrene in urine in view of acceptable occupational exposure to polycyclic aromatic hydrocarbons", *Toxicol. Lett*., **231**(2), 239-248. https://doi.org/10.1016/j.toxlet.2014.05.001.

Kim, K.H., Jahan, S.A., Kabir, E. and Brown, R.J.J.E.I. (2013), "A review of airborne polycyclic aromatic hydrocarbons (PAHs) and their human health effects", *Environ. Int*., **60**, 71-80. https://doi.org/10.1016/j.envint.2013.07.019.

Kumar, V., George, P., Singh, R.K., Chowdhury, P.J.M. and Treatment, W. (2021), "Enhanced transport of Lignosulfonate by integrating adsorption sweep in a liquid membrane module", *Membr. Water Treat.*, **12**(3), 95-106. https://doi.org/10.12989/mwt.2021.12.3.095.

Li, D., Cao, X., Zhang, Q., Ren, X., Jiang, L., Li, D., Deng, W. and Liu, H. (2019a), "Facile in situ synthesis of core–shell MOF@Ag nanoparticle composites on screen-printed electrodes for ultrasensitive SERS detection of polycyclic aromatic

hydrocarbons", *J. Mater. Chem. A.*, **7**(23), 14108-14117. https://doi.org/10.1039/C9TA03690C.

Li, H., Han, W., Lv, R., Zhai, A., Li, X.L., Gu, W. and Liu, X. (2019b), "Dual-function mixed-lanthanide metal–organic framework for ratiometric water detection in bioethanol and temperature sensing", *Anal. Chem*., **91**(3), 2148-2154. https://doi.org/10.1021/acs.analchem.8b04690.

Li, J., Yuan, S., Qin, J.-S., Pang, J., Zhang, P., Zhang, Y., Huang, Y., Drake, H.F., Liu, W.R. and Zhou, H.C. (2020a), "Stepwise assembly of turn-on fluorescence sensors in multicomponent metal–organic frameworks for in vitro cyanide detection", *Angew. Chem. Int. Edit*., **59**(24), 9319-9323. https://doi.org/10.1002/anie.202000702.

Li, C., Zeng, C., Chen, Z., Jiang, Y., Yao, H., Yang, Y. and Wong, W.T. (2020b), "Luminescent lanthanide metal-organic framework test strip for immediate detection of tetracycline antibiotics in water", *J. Hazard. Mater*., **384**, 121498. https://doi.org/10.1016/j.jhazmat.2019.121498

Li, Y., Li, Y., Wang, Y., Ma, G., Liu, X., Li, Y. and Soar, J. (2020c), "Application of zeolitic imidazolate frameworks (ZIF-8)/ionic liquid composites modified nano-carbon paste electrode as sensor for electroanalytical sensing of 1-hydroxypyrene", *Microchem. J*., **159**, 105433. https://doi.org/10.1016/j.microc.2020.105433.

Li, Z., Cao, Y., Qin, H., Ma, Y., Pan, L. and Sun, J. (2022), "Integration of chemical and biological methods: A case study of polycyclic aromatic hydrocarbons pollution monitoring in Shandong Peninsula, China", *J. Environ. Sci*., **111**, 24-37. https://doi.org/10.1016/j.jes.2021.02.025.

Liang, Q., Jiao, X., Yan, Y., Xie, Z., Lu, G., Liu, J. and Han, Y.J.A.F.M. (2019), "Separating crystallization process of P3HT and O-IDTBR to construct highly crystalline interpenetrating network with optimized vertical phase separation", *Adv. Funct. Mater.* **29**(47), 1807591. https://doi.org/10.1002/adfm.201807591.

Liang, Z., Li, M., Wang, Q., Qin, Y., Stuard, S.J., Peng, Z., Deng, Y., Ade, H., Ye, L. and Geng, Y. (2020), "Optimization requirements of efficient polythiophene: Nonfullerene organic solar cells", *Joule*, **4**(6), 1278-1295. https://doi.org/10.1016/j.joule.2020.04.014.

Lin, R.B., Liu, S.Y., Ye, J.W., Li, X.Y. and Zhang, J.P.J.A.S. (2016), "Photoluminescent metal–organic frameworks for gas sensing", *Adv. Sci*., **3**(7), 1500434. https://doi.org/10.1002/advs.201500434.

Lin, Y., Gao, X., Qiu, X., Liu, J., Tseng, C.-H., Zhang, J.J., Araujo, J.A. and Zhu, Y. (2021), "Urinary carboxylic acid metabolites as possible novel biomarkers of exposures to alkylated polycyclic aromatic hydrocarbons", *Environ. Int*., **147**, 106325. https://doi.org/10.1016/j.envint.2020.106325

Liu, C.Y., Chen, X.R., Chen, H.X., Niu, Z., Hirao, H., Braunstein, P. and Lang, J.P. (2020), "Ultrafast luminescent light-up guest detection based on the lock of the host molecular vibration", *J. Am. Chem. Soc*., **142**(14), 6690-6697. https://doi.org/10.1021/jacs.0c00368.

Liu, Y., Xian, K., Peng, Z., Gao, M., Shi, Y., Deng, Y., Geng, Y. and Ye, L. (2021), "Tuning the molar mass of P3HT via direct arylation polycondensation yields optimal interaction and high efficiency in nonfullerene organic solar cells", *J. Mater. Chem. A*, **9**(35), 19874-19885. https://doi.org/10.1039/D1TA02253A.

Luo, T.Y., Das, P., White, D.L., Liu, C., Star, A. and Rosi, N.L. (2020), "Turn-On" detection of gossypol using Ln3+-based metal–organic frameworks and Ln3+ salts", *J. Am. Chem. Soc*., **142**(6), 2897-2904. https://doi.org/10.1021/jacs.9b11429.

Ma, J., Li, S., Wu, G., Wang, S., Guo, X., Wang, L., Wang, X., Li, J. and Chen, L. (2019), "v (vinylidene fluoride) for use in determination of sulfonylurea herbicides in aqueous environments by high performance liquid chromatography", *J. Colloid Interf. Sci*., **553**, 834-844. https://doi.org/10.1016/j.jcis.2019.06.082.

Mallick, A., El-Zohry, A.M., Shekhah, O., Yin, J., Jia, J., Aggarwal, H., Emwas, A.H., Mohammed, O.F. and Eddaoudi, M. (2019), "Unprecedented ultralow detection limit of amines using a thiadiazole-functionalized Zr (IV)-based metal–organic framework", *J. Am. Chem. Soc*., **141**(18), 7245-7249. https://doi.org/10.1021/jacs.9b01839

Mattarozzi, M., Musci, M., Careri, M., Mangia, A., Fustinoni, S., Campo, L. and Bianchi, F.J.J.O.C.A. (2009), "A novel headspace solid-phase microextraction method using in situ derivatization and a diethoxydiphenylsilane fibre for the gas chromatography–mass spectrometry determination of urinary hydroxy polycyclic aromatic hydrocarbons", *J. Chromatogr. A*, **1216**(30), 5634-5639. https://doi.org/10.1016/j.chroma.2009.05.072.

Oliveira, M., Slezakova, K., Delerue-Matos, C., Pereira, M.C. and Morais, S. (2019), "Children environmental exposure to particulate matter and polycyclic aromatic hydrocarbons and biomonitoring in school environments: A review on indoor and outdoor exposure levels, major sources and health impacts", *Environ. Int*., **124**, 180-204. https://doi.org/10.1016/j.envint.2018.12.052

Omidi, F., Khadem, M., Dehghani, F., Seyedsomeah, M. and Shahtaheri, S.J. (2020), "Ultrasound-assisted dispersive micro-solid-phase extraction based on N-doped mesoporous carbon and high-performance liquid chromatographic determination of 1-hydroxypyrene in urine samples", *J. Sep. Sci*., **43**(13), 2602-2609. https://doi.org/10.1002/jssc.202000172.

Ou, Q., Tawfik, S.M., Zhang, X. and Lee, Y.I. (2020), "Novel "turn on–off" paper sensor based on nonionic conjugated polythiophene-coated CdTe QDs for efficient visual detection of cholinesterase activity", *Analyst*, **145**(12), 4305-4313. https://doi.org/10.1039/D0AN00924E

Pang, Y., Huang, Y., Li, W., Feng, L. and Shen, X. (2019a), "Conjugated polyelectrolyte/graphene multilayer films for simultaneous electrochemical sensing of three monohydroxylated polycyclic aromatic hydrocarbons", *ACS Appl. Nano Mater*., **2**(12), 7785-7794. https://doi.org/10.1021/acsanm.9b01821.

Pang, Y., Zhang, Y., Sun, X., Ding, H., Ma, T. and Shen, X. (2019b), "Synergistical accumulation for electrochemical sensing of 1-hydroxypyrene on electroreduced graphene oxide electrode", *Talanta*, **192**, 387-394. https://doi.org/10.1016/j.talanta.2018.08.042.

Pang, Y.H., Huang, Y.Y., Li, W.Y., Yang, N.C. and Shen, X.F. (2020a), "Electrochemical detection of three monohydroxylated polycyclic aromatic hydrocarbons using electroreduced graphene oxide modified screen-printed electrode", *Electroanalysis*, **32**(7), 1459-1467. https://doi.org/10.1002/elan.201900692.

Pang, Y., Yang, N., Shen, X., Zhang, Y. and Feng, L. (2020b), "Conjugated polymer self-assembled with graphene: Synthesis and electrochemical 1-hydroxypyrene sensor", *Polymer,* **188**, 122139. https://doi.org/10.1016/j.polymer.2019.122139.

Phan-Quang, G.C., Yang, N., Lee, H.K., Sim, H.Y.F., Koh, C.S.L., Kao, Y.C., Wong, Z.C., Tan, E.K.M., Miao, Y.E., Fan, W., Liu, T., Phang, I.Y. and Ling, X.Y. (2019), "Tracking airborne molecules from Afar: Three-dimensional metal–organic framework-surface-enhanced Raman scattering platform for stand-off and real-time atmospheric monitoring", *ACS Nano*, **13**(10), 12090-12099. https://doi.org/10.1021/acsnano.9b06486.

Phaomei, G. and Yaiphaba, N.J.A.I.N.R. (2015), "Ce3+ sensitize RE3+ (RE= Dy, Tb, Eu, Sm) doped LaPO4 nanophosphor with white emission tunability", *Adv. Nano Res.*, **3**(2), 55-66. http://doi.org/10.12989/anr.2015.3.2.055.

Pruneda-Álvarez, L.G., Pérez-Vázquez, F.J., Ruíz-Vera, T., Ochoa-Martínez, Á.C., Orta-García, S.T., Jiménez-Avalos, J.A., Pérez-Maldonado, I.N.J.E.S. and Research, P. (2016), "Urinary 1-hydroxypyrene concentration as an exposure biomarker to polycyclic aromatic hydrocarbons (PAHs) in Mexican women from different hot spot scenarios and health risk assessment", *Environ. Sci. Pollut. Res. Int.*, **23**(7), 6816-6825. https://doi.org/10.1007/s11356-015-5918-

Nsibande, S.A. and Forbes, P.B.C. (2020), "Development of a turn-on graphene quantum dot-based fluorescent probe for sensing of pyrene in water", *RSC Adv.*, **10**(21), 12119-12128. https://doi.org/10.1039/C9RA10153E.

Sava Gallis, D.F., Vogel, D.J., Vincent, G.A., Rimsza, J.M. and Nenoff, T.M. (2019), "NOx Adsorption and Optical Detection in Rare Earth Metal–Organic Frameworks", *ACS Appl. Mater. Interf.*, **11**(46), 43270-43277. https://doi.org/10.1021/acsami.9b16470

Serrano, M., Bartolome, M., Gallego-Pico, A., Garcinuno, R., Bravo, J. and Fernandez, P.J.T. (2015), "Synthesis of a molecularly imprinted polymer for the isolation of 1-hydroxypyrene in human urine", *Talanta*, **143** 71-76. https://doi.org/10.1016/j.talanta.2015.04.092.

Serrano, M., Bartolomé, M., Bravo, J.C., Paniagua, G., Gañan, J., Gallego-Picó, A. and Garcinuño, R.M.J.T. (2017), "On-line flow injection molecularly imprinted solid phase extraction for the preconcentration and determination of 1-hydroxypyrene in urine samples", *Talanta*, **166** 375-382. https://doi.org/10.1016/j.talanta.2016.01.048.

Shen, X., Cui, Y., Pang, Y. and Qian, H. (2012a), "Pre-concentration and in situ electrochemical sensing of 1-hydroxypyrene on an electrodeposited poly(3-methylthiophene) film modified electrode", *J. Electroanal. Chem.*, **667**, 1-6. https://doi.org/10.1016/j.jelechem.2011.12.016.

Shen, X., Cui, Y., Pang, Y. and Qian, H.J.E.A. (2012b), "Graphene oxide nanoribbon and polyhedral oligomeric silsesquioxane assembled composite frameworks for pre-concentrating and electrochemical sensing of 1-hydroxypyrene", *Electrochim. Acta*, **59**, 91-99. https://doi.org/10.1016/j.electacta.2011.10.037.

Shim, J., Tawfik, S.M., Thangadurai, D.T. and Lee, Y.-I. (2021), "Amphiphilic conjugated polythiophene-based fluorescence "Turn on" sensor for selective detection of Escherichia coli in water and milk", *Bull. Korean Chem. Soc.*, **42**(7), 1047-1053. https://doi.org/10.1002/bkcs.12333.

Song, X.Z., Song, S.Y., Zhao, S.N., Hao, Z.M., Zhu, M., Meng, X., Wu, L.L. and Zhang, H.J.J.A.F.M. (2014), "Single-Crystal-to-Single-Crystal transformation of a europium (III) metal–organic framework producing a multi-responsive luminescent sensor", *Adv. Funct. Mater.*, **24**(26), 4034-4041. https://doi.org/10.1002/adfm.201303986.

Soury, S., Bahrami, A., Alizadeh, S., Ghorbani Shahna, F. and Nematollahi, D. (2019), "Development of a needle trap device packed with zinc based metal-organic framework sorbent for the sampling and analysis of polycyclic aromatic hydrocarbons in the air", *Microchem. J.*, **148**, 346-354. https://doi.org/10.1016/j.microc.2019.05.019.

Sun, C.Z., Zhang, L.Y., Wang, J.Y., Chen, Z.N. and Dai, F.R. (2018), "Sensitive and selective urinary 1-hydroxypyrene detection by dinuclear terbium-sulfonylcalixarene complex", *Dalton Transact.*, **47**(25), 8301-8306. https://doi.org/10.1039/C8DT01604F.

Sur, U.K.J.A.i.n.r. (2013), "Surface-enhanced Raman scattering (SERS) spectroscopy: a versatile spectroscopic and analytical technique used in nanoscience and nanotechnology", *Adv. Nano Res.*, **1**(2), 111-124. https://doi.org/10.12989/anr.2013.1.2.111.

Tawfik, S.M., Huy, B.T., Sharipov, M., Abd-Elaal, A. and Lee, Y.-I. (2018a), "Enhanced fluorescence of CdTe quantum dots capped with a novel nonionic alginate for selective optosensing of ibuprofen", *Sensor Actuat. B Chem.*, **256**, 243-250. https://doi.org/10.1016/j.snb.2017.10.092.

Tawfik, S.M., Shim, J., Biechele-Speziale, D., Sharipov, M. and Lee, Y.I. (2018b), "Novel "turn off-on" sensors for highly selective and sensitive detection of spermine based on heparin-quenching of fluorescence CdTe quantum dots-coated amphiphilic thiophene copolymers", *Sensors Actuat. B Chem.*, **257**, 734-744. https://doi.org/10.1016/j.snb.2017.10.172.

Tawfik, S.M., Sharipov, M., Kakhkhorov, S., Elmasry, M.R. and Lee, Y.I. (2019), "Multiple emitting amphiphilic conjugated polythiophenes-coated CdTe QDs for picogram detection of trinitrophenol explosive and application using chitosan film and paper-based sensor coupled with smartphone", *Adv. Sci.*, **6**(2), 1801467. https://doi.org/10.1002/advs.201801467.

Tawfik, S.M., Elmasry, M.R., Sharipov, M., Azizov, S., Lee, C.H. and Lee, Y.I. (2020), "Dual emission nonionic molecular imprinting conjugated polythiophenes-based paper devices and their nanofibers for point-of-care biomarkers detection", *Biosens. Bioelectron.*, **160**, 112211. https://doi.org/10.1016/j.bios.2020.112211.

Tropp, J., Ihde, M.H., Williams, A.K., White, N.J., Eedugurala, N., Bell, N.C., Azoulay, J.D. and Bonizzoni, M. (2019), "A sensor array for the discrimination of polycyclic aromatic hydrocarbons using conjugated polymers and the inner filter effect", *Chem. Sci.*, **10**(44), 10247-10255. https://doi.org/10.1039/C9SC03405F.

Wang, Y., Wong, L.Y., Meng, L., Pittman, E.N., Trinidad, D.A., Hubbard, K.L., Etheredge, A., Del Valle-Pinero, A.Y., Zamoiski, R., van Bemmel, D.M., Borek, N., Patel, V., Kimmel, H.L., Conway, K.P., Lawrence, C., Edwards, K.C., Hyland, A., Goniewicz, M.L., Hatsukami, D., Hecht, S.S. and Calafat, A.M. (2019), "Urinary concentrations of monohydroxylated polycyclic aromatic hydrocarbons in adults from the U.S. Population Assessment of Tobacco and Health (PATH) Study Wave 1 (2013–2014)", *Environ. Int.*, **123**, 201-208. https://doi.org/10.1016/j.envint.2018.11.068.

Wang, Q., Qin, Y., Li, M., Ye, L. and Geng, Y. (2020), "Molecular engineering and morphology control of polythiophene: Nonfullerene acceptor blends for high-performance solar cells", *Adv. Energy Mater.*, **10**(45), 2002572. https://doi.org/10.1002/aenm.202002572.

Wang, Q., Li, M., Peng, Z., Kirby, N., Deng, Y., Ye, L. and Geng, Y. (2021), "Calculation aided miscibility manipulation enables highly efficient polythiophene:nonfullerene photovoltaic cells", *Sci. China Chem.*, **64**(3), 478-487. https://doi.org/10.1007/s11426-020-9890-6.

Wu, G., Ma, J., Wang, S., Chai, H., Guo, L., Li, J., Ostovan, A., Guan, Y. and Chen, L. (2020), "Cationic metal-organic framework based mixed-matrix membrane for extraction of phenoxy carboxylic acid (PCA) herbicides from water samples followed by UHPLC-MS/MS determination", *J. Hazard. Mater.*, **394**, 122556. https://doi.org/10.1016/j.jhazmat.2020.122556.

Wu, S., Min, H., Shi, W. and Cheng, P. (2020), "Multicenter metal–organic framework-based ratiometric fluorescent sensors", *Adv. Mater.* **32**(3), 1805871. https://doi.org/10.1002/adma.201805871.

Xu, X.Y., Lian, X., Hao, J.N., Zhang, C. and Yan, B.J.A.M. (2017a), "A double-stimuli-responsive fluorescent center for monitoring of food spoilage based on dye covalently modified EuMOFs: From sensory hydrogels to logic devices", *Adv. Mater.* **29**(37), 1702298. https://doi.org/10.1002/adma.201702298.

Xu, X.Y. and Yan, B.J.A.F.M. (2017b), "Intelligent molecular searcher from logic computing network based on Eu (III) functionalized UMOFs for environmental monitoring", *Adv. Funct. Mater.* **27**(23), 1700247.

https://doi.org/10.1002/adfm.201700247.
Xue, J.H., Xiao, K.P., Wang, Y.S., Liu, L., Li, J.Q., Li, M., Qu, Y.N. and Xiao, X.L. (2020), "Aggregation-induced photoluminescence enhancement of protamine-templated gold nanoclusters for 1-hydroxypyrene detection using 9-hydroxyphenanthrene as a sensitizer", *Colloid Surf. B*, **189**, 110873. https://doi.org/10.1016/j.colsurfb.2020.110873.
Yang, M., Wang, Y., Ren, J., Li, M., Wang, Q., Li, N., Zhu, J. and Zou, X. (2019), "A rapid and sensitive method of determination of 1-hydroxypyrene glucuronide in urine by UPLC–FLD", *Chromatographia*, **82**(5), 835-842. https://doi.org/10.1007/s10337-019-03713-0
Zeng, X., Hu, J., Zhang, M., Wang, F., Wu, L. and Hou, X. (2020), "Visual detection of fluoride anions using mixed lanthanide metal–organic frameworks with a smartphone", *Anal. Chem*., **92**(2), 2097-2102. https://doi.org/10.1021/acs.analchem.9b04598.
Zhang, Z.X., Zhu, Y.X. and Zhang, Y.J.T. (2015), "Simultaneous determination of 9-ethylphenanthrene, pyrene and 1-hydroxypyrene in an aqueous solution by synchronous fluorimetry using the double scans method and hydroxyl-propyl beta-cyclodextrin as a sensitizer", *Talanta*, **144**, 836-843. https://doi.org/10.1016/j.talanta.2015.05.067.
Zhang, F., Yao, H., Chu, T., Zhang, G., Wang, Y. and Yang, Y.J.C.A.E.J. (2017a), "A lanthanide MOF thin-film fixed with Co_3O_4 nano-anchors as a highly efficient luminescent sensor for nitrofuran antibiotics", *Chem. Eur. J*., **23**(43), 10293-10300. https://doi.org/10.1002/chem.201701852.
Zhang, K., Xie, X., Li, H., Gao, J., Nie, L., Pan, Y., Xie, J., Tian, D., Liu, W. and Fan, Q.J.A.M. (2017b), "Highly water-stable lanthanide–oxalate MOFs with remarkable proton conductivity and tunable luminescence", *Adv. Mater*., **29**(34), 1701804. https://doi.org/10.1002/adma.201701804.
Zhou, J., Li, H., Zhang, H., Li, H., Shi, W. and Cheng, P.J.A.M. (2015), "A bimetallic lanthanide metal–organic material as a self-calibrating color-gradient luminescent sensor", *Adv. Mater.*, **27**(44), 7072-7077. https://doi.org/10.1002/adma.201502760.
Zhou, Y., Yang, Q., Cuan, J., Wang, Y., Gan, N., Cao, Y. and Li, T. (2018), "A pyrene-involved luminescent MOF for monitoring 1-hydroxypyrene, a biomarker for human intoxication of PAH carcinogens", *Analyst*, **143**(15), 3628-3634. https://doi.org/10.1039/C8AN00909K.
Zhou, H.Q., He, Y., Hu, J.Y., Chung, L.H., Gu, Q., Liao, W.M., Zeller, M., Xu, Z. and He, J. (2021), "Conjugated crosslinks boost the conductivity and stability of a single crystalline metal–organic framework", *Chem. Commun*., **57**(2), 187-190. https://doi.org/10.1039/D0CC06765B.